

University of Dundee

**Loss-of-function mutations of CUL3, a high confidence gene for psychiatric disorders, lead to aberrant neurodevelopment in human induced pluripotent stem cells**

Fischer, Sandra; Schlotthauer, Ines; Kizner, Valeria; Macartney, Thomas; Dorner-Ciossek, Cornelia; Gillardon, Frank

*Published in:*  
Neuroscience

*DOI:*  
[10.1016/j.neuroscience.2020.08.028](https://doi.org/10.1016/j.neuroscience.2020.08.028)

*Publication date:*  
2020

*Licence:*  
CC BY-NC-ND

*Document Version*  
Peer reviewed version

[Link to publication in Discovery Research Portal](#)

*Citation for published version (APA):*

Fischer, S., Schlotthauer, I., Kizner, V., Macartney, T., Dorner-Ciossek, C., & Gillardon, F. (2020). Loss-of-function mutations of CUL3, a high confidence gene for psychiatric disorders, lead to aberrant neurodevelopment in human induced pluripotent stem cells. *Neuroscience*, *448*, 234-254. <https://doi.org/10.1016/j.neuroscience.2020.08.028>

**General rights**

Copyright and moral rights for the publications made accessible in Discovery Research Portal are retained by the authors and/or other copyright owners and it is a condition of accessing publications that users recognise and abide by the legal requirements associated with these rights.

- Users may download and print one copy of any publication from Discovery Research Portal for the purpose of private study or research.
- You may not further distribute the material or use it for any profit-making activity or commercial gain.
- You may freely distribute the URL identifying the publication in the public portal.

**Take down policy**

If you believe that this document breaches copyright please contact us providing details, and we will remove access to the work immediately and investigate your claim.

## Journal Pre-proofs

Loss-of-function mutations of CUL3, a high confidence gene for psychiatric disorders, lead to aberrant neurodevelopment in human induced pluripotent stem cells

Sandra Fischer, Ines Schlotthauer, Valeria Kizner, Thomas Macartney, Cornelia Dorner-Ciossek, Frank Gillardon

PII: S0306-4522(20)30545-5  
DOI: <https://doi.org/10.1016/j.neuroscience.2020.08.028>  
Reference: NSC 19845

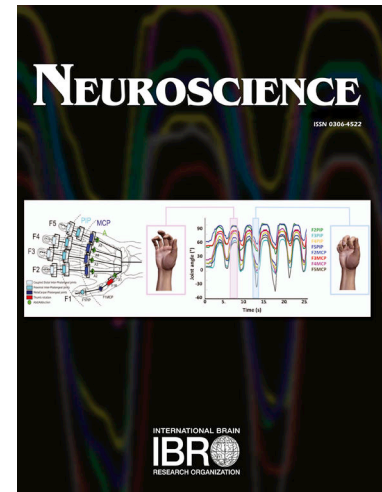
To appear in: *Neuroscience*

Received Date: 16 March 2020  
Revised Date: 25 July 2020  
Accepted Date: 20 August 2020

Please cite this article as: S. Fischer, I. Schlotthauer, V. Kizner, T. Macartney, C. Dorner-Ciossek, F. Gillardon, Loss-of-function mutations of CUL3, a high confidence gene for psychiatric disorders, lead to aberrant neurodevelopment in human induced pluripotent stem cells, *Neuroscience* (2020), doi: <https://doi.org/10.1016/j.neuroscience.2020.08.028>

This is a PDF file of an article that has undergone enhancements after acceptance, such as the addition of a cover page and metadata, and formatting for readability, but it is not yet the definitive version of record. This version will undergo additional copyediting, typesetting and review before it is published in its final form, but we are providing this version to give early visibility of the article. Please note that, during the production process, errors may be discovered which could affect the content, and all legal disclaimers that apply to the journal pertain.

© 2020 Published by Elsevier Ltd on behalf of IBRO. This manuscript version is made available under the CC-BY-NC-ND 4.0 license <http://creativecommons.org/licenses/by-nc-nd/4.0/>.



**Supplementary Table S2.** Summary of statistical analysis

Figure	Experiment	Test used	Statistic's value	P value
1B	CUL3 mRNA expression	Welch's ANOVA	W(4.00, 11.91) = 35.37	
	+/+ <sub>4</sub> vs. +/- <sub>6</sub>	Welch's t-test	t(8.15) = 5.27	0.0007
	+/+ <sub>2</sub> vs. +/- <sub>6</sub>	Welch's t-test	t(6.21) = 5.42	0.0015
	+/+ <sub>13</sub> vs. +/- <sub>6</sub>	Welch's t-test	t(9.82) = 4.26	0.0017
	+/+ <sub>4</sub> vs. +/- <sub>19</sub>	Welch's t-test	t(9.91) = 10.08	<0.0001
	+/+ <sub>2</sub> vs. +/- <sub>19</sub>	Welch's t-test	t(7.63) = 11.48	<0.0001
	+/+ <sub>13</sub> vs. +/- <sub>19</sub>	Welch's t-test	t(7.96) = 7.03	0.0001
2C	Cullin-3 protein expression	Welch's ANOVA	W(4.00, 7.32) = 6.31	
	+/+ <sub>4</sub> vs. +/- <sub>6</sub>	Welch's t-test	t(4.17) = 4.77	0.0080
	+/+ <sub>2</sub> vs. +/- <sub>6</sub>	Welch's t-test	t(5.27) = 4.27	0.0071
	+/+ <sub>13</sub> vs. +/- <sub>6</sub>	Welch's t-test	t(6.00) = 4.17	0.0059
	+/+ <sub>4</sub> vs. +/- <sub>19</sub>	Welch's t-test	t(5.30) = 3.05	0.0265
	+/+ <sub>2</sub> vs. +/- <sub>19</sub>	Welch's t-test	t(6.00) = 2.50	0.0469
	+/+ <sub>13</sub> vs. +/- <sub>19</sub>	Welch's t-test	t(5.16) = 2.60	0.0469
5A	PAX6 mRNA expression	Welch's ANOVA	W(4.00, 4.51) = 316.7	
	+/+ <sub>4</sub> vs. +/- <sub>6</sub>	Welch's t-test	t(2.20) = 34.92	0.0005
	+/+ <sub>2</sub> vs. +/- <sub>6</sub>	Welch's t-test	t(2.03) = 34.85	0.0007
	+/+ <sub>13</sub> vs. +/- <sub>6</sub>	Welch's t-test	t(2.14) = 38.48	0.0004
	+/+ <sub>4</sub> vs. +/- <sub>19</sub>	Welch's t-test	t(2.05) = 12.52	0.0057
	+/+ <sub>2</sub> vs. +/- <sub>19</sub>	Welch's t-test	t(2.01) = 12.17	0.0066
	+/+ <sub>13</sub> vs. +/- <sub>19</sub>	Welch's t-test	t(2.04) = 14.28	0.0045
5B	SLC1A3 mRNA expression	Welch's ANOVA	W(4.00, 4.67) = 5567	
	+/+ <sub>4</sub> vs. +/- <sub>6</sub>	Welch's t-test	t(2.01) = 21.98	0.0020
	+/+ <sub>2</sub> vs. +/- <sub>6</sub>	Welch's t-test	t(2.02) = 20.51	0.0022
	+/+ <sub>13</sub> vs. +/- <sub>6</sub>	Welch's t-test	t(2.00) = 21.15	0.0022
	+/+ <sub>4</sub> vs. +/- <sub>19</sub>	Welch's t-test	t(3.86) = 156.6	<0.0001
	+/+ <sub>2</sub> vs. +/- <sub>19</sub>	Welch's t-test	t(3.52) = 98.39	<0.0001
	+/+ <sub>13</sub> vs. +/- <sub>19</sub>	Welch's t-test	t(2.86) = 168.4	<0.0001
5C	Pax-6 positive cells	Welch's ANOVA	W(4.00, 4.42) = 41.98	
	+/+ <sub>4</sub> vs. +/- <sub>6</sub>	Welch's t-test	t(2.03) = 10.10	0.0092
	+/+ <sub>2</sub> vs. +/- <sub>6</sub>	Welch's t-test	t(2.00) = 10.54	0.0088
	+/+ <sub>13</sub> vs. +/- <sub>6</sub>	Welch's t-test	t(2.01) = 10.38	0.0090
	+/+ <sub>4</sub> vs. +/- <sub>19</sub>	Welch's t-test	t(2.61) = 8.13	0.0064
	+/+ <sub>2</sub> vs. +/- <sub>19</sub>	Welch's t-test	t(2.06) = 10.63	0.0079
	+/+ <sub>13</sub> vs. +/- <sub>19</sub>	Welch's t-test	t(2.30) = 9.65	0.0066
6A	MEA spike rate	two-way ANOVA		
		Interaction	F(2, 341) = 12.40	
		Row factor	F(2, 341) = 5.43	
		Column factor	F(1, 341) = 38.62	
	+/+ <sub>div19</sub> vs. +/- <sub>div19</sub>	Welch's t-test	t(56.35) = 5.11	<0.0001
+/+ <sub>div23</sub> vs. +/- <sub>div23</sub>	Welch's t-test	t(48.39) = 6.64	<0.0001	

**Supplementary Table S2.** Summary of statistical analysis (continued)

Figure	Experiment	Test used	Statistic's value	P value
8	Number of rosettes	Kruskal-Wallis	KW(5) = 214.9	
	+/+ <sub>4</sub> vs. +/- <sub>6</sub>	Mann-Whitney U	U(50,47) = 25	<0.0001
	+/+ <sub>2</sub> vs. +/- <sub>6</sub>	Mann-Whitney U	U(50,47) = 25	<0.0001
	+/+ <sub>13</sub> vs. +/- <sub>6</sub>	Mann-Whitney U	U(50,47) = 25	<0.0001
	+/+ <sub>4</sub> vs. +/- <sub>19</sub>	Mann-Whitney U	U(50,48) = 225	<0.0001
	+/+ <sub>2</sub> vs. +/- <sub>19</sub>	Mann-Whitney U	U(50,48) = 225	<0.0001
	+/+ <sub>13</sub> vs. +/- <sub>19</sub>	Mann-Whitney U	U(50,48) = 225	<0.0001
9B	Syn-1/2 positive puncta	Welch's ANOVA	W(4.00, 1197) = 760.8	
	+/+ <sub>4</sub> vs. +/- <sub>6</sub>	Welch's t-test	t(719.1) = 33.45	<0.0001
	+/+ <sub>2</sub> vs. +/- <sub>6</sub>	Welch's t-test	t(704.2) = 33.98	<0.0001
	+/+ <sub>13</sub> vs. +/- <sub>6</sub>	Welch's t-test	t(810.3) = 43.33	<0.0001
	+/+ <sub>4</sub> vs. +/- <sub>19</sub>	Welch's t-test	t(932.2) = 17.37	<0.0001
	+/+ <sub>2</sub> vs. +/- <sub>19</sub>	Welch's t-test	t(924.4) = 16.73	<0.0001
	+/+ <sub>13</sub> vs. +/- <sub>19</sub>	Welch's t-test	t(1033) = 23.97	<0.0001
10B	MEA spike rate	two-way ANOVA		
		Interaction	F (2, 102) = 8.224	
		Row factor	F (2, 102) = 215.3	
		Column factor	F (1, 102) = 25.28	
	+/+ <sub>2</sub> mA vs. +/- <sub>2</sub> mA	Welch's t-test	t(21.09) = 3.09	0.0056
+/+ <sub>5</sub> mA vs. +/- <sub>5</sub> mA	Welch's t-test	t(23.93) = 4.07	0.0004	
10C	Calcium imaging	two-way ANOVA		
		Interaction	F (4, 110) = 6.289	
		Row factor	F (4, 110) = 248.5	
		Column factor	F (1, 110) = 85.62	
	+/+ <sub>2</sub> Hz vs. +/- <sub>2</sub> Hz	Welch's t-test	t(20.61) = 4.18	0.0004
	+/+ <sub>5</sub> Hz vs. +/- <sub>5</sub> Hz	Welch's t-test	t(18.58) = 4.36	0.0004
	+/+ <sub>10</sub> Hz vs. +/- <sub>10</sub> Hz	Welch's t-test	t(18.25) = 4.92	0.0001
	+/+ <sub>20</sub> Hz vs. +/- <sub>20</sub> Hz	Welch's t-test	t(19.10) = 4.81	0.0001
+/+ <sub>50</sub> Hz vs. +/- <sub>50</sub> Hz	Welch's t-test	t(20.32) = 4.61	0.0002	
11B	mRNA expression			
	+/+ <sub>SPRY1</sub> vs. +/- <sub>SPRY1</sub>	Welch's t-test	t(28.81) = 3.36	0.0022
	+/+ <sub>IL17RD</sub> vs. +/- <sub>IL17RD</sub>	Welch's t-test	t(29.56) = 2.83	0.0083

**Supplementary Table S1.** Primary antibodies used for immunocytochemistry (ICC) or immunoblotting (IB).

Name	Species	Clonality	Dilution	Supplier	Cat. No.
Anti-Cullin-3	Mouse	Monoclonal	1:200 IB	Santa Cruz, Dallas, TX, USA	sc-166110
Anti-Cullin-3	Goat	Polyclonal	1:200 IB	Santa Cruz, Dallas, TX, USA	sc-8556

Anti-beta-Actin	Mouse	Monoclonal	1:3000 IB	Sigma-Aldrich, St. Louis, MO, USA	A5316
Anti-Oct-4	Rabbit	Monoclonal	1:400 ICC	Cell Signaling Technology, Danvers, MA, USA	2840
Anti-Tra-1-60	Mouse	Monoclonal	1:100 ICC	STEMCELL, Vancouver, Canada	60064
Anti-Pax-6	Rabbit	Polyclonal	1:100 ICC	Thermo Fisher Scientific, Waltham, MA, USA	42-6600
Anti-Map-2	Chicken	Polyclonal	1:1000 ICC	EnCor Biotechnology, Gainesville, FL, USA	CPCA-MAP2
Anti-vGlut-1	Mouse	Monoclonal	1:1000 ICC	Synaptic Systems, Goettingen, Germany	135511
Anti-Syn-1/2	Rabbit	Polyclonal	1:5000 ICC	Synaptic Systems, Goettingen, Germany	106002
Anti-Psd-95	Mouse	Monoclonal	1:100 ICC	Thermo Fisher Scientific, Waltham, MA, USA	MA1-046
Anti-RhoA	Mouse	Monoclonal	1:250 IB	Cytoskeleton, Denver, CO, USA	ARH04

1 **Loss-of-function mutations of CUL3, a high confidence gene for psychiatric**  
2 **disorders, lead to aberrant neurodevelopment in human induced pluripotent**  
3 **stem cells**

4

5 Sandra Fischer<sup>1,\*</sup>, Ines Schlotthauer<sup>1,\*</sup>, Valeria Kizner<sup>1</sup>, Thomas Macartney<sup>2</sup>, Cornelia Dorner-  
6 Ciossek<sup>1</sup>, and Frank Gillardon<sup>1</sup>

7

8 <sup>1</sup>CNS Diseases Research, Boehringer Ingelheim Pharma GmbH & Co. KG, 88397 Biberach  
9 an der Riss, Germany

10 <sup>2</sup>MRC Protein Phosphorylation and Ubiquitylation Unit, Sir James Black Centre, University of  
11 Dundee, Dundee DD1 5EH, UK

12 \*These authors contributed equally

13

14 **Corresponding author:**

15 Prof. Frank Gillardon, CNS Diseases Research, Boehringer Ingelheim Pharma GmbH & Co.  
16 KG, Birkendorfer Str. 65, 88397 Biberach an der Riss, Germany. Telephone: +49-7351-  
17 548460; e-mail: [frank.gillardon@boehringer-ingelheim.com](mailto:frank.gillardon@boehringer-ingelheim.com)

18

19

20 **Funding information**

21 The research leading to these results has received support (one iPSC line from a healthy donor)  
22 from the Innovative Medicines Initiative Joint Undertaking under grant agreement n° 115439.  
23 Resources are composed of financial contribution from the European Union's Seventh  
24 Framework Program (FP7/2007-2013) and in kind contributions from EFPIA companies. This  
25 publication reflects only the author's views and neither the Innovative Medicines Initiative Joint  
26 Undertaking nor EFPIA nor the European Commission are liable for any use that may be made  
27 of the information contained therein.

28

29 **Declarations of interest**

30 Boehringer Ingelheim Pharma GmbH & Co. KG supported this work only by providing financial  
31 support in the form of authors' salaries and research materials. Study design, data analysis,  
32 decision to publish, and writing of the manuscript was performed independently. All authors  
33 declare no potential conflicts of interest.

34

**Abstract**

Both rare, high risk, loss-of-function mutations and common, low risk, genetic variants in the CUL3 gene are strongly associated with neuropsychiatric disorders. Network analyses of neuropsychiatric risk genes have shown high CUL3 expression in the prenatal human brain and an enrichment in neural precursor cells (NPCs) and cortical neurons. The role of CUL3 in human neurodevelopment however, is poorly understood. In the present study, we used CRISPR/Cas9 nickase to knockout CUL3 in human induced pluripotent stem cells (iPSCs). iPSCs were subsequently differentiated into cortical glutamatergic neurons using two different protocols and tested for structural/functional alterations. Immunocytochemical analysis and transcriptomic profiling revealed that pluripotency of heterozygous CUL3 knockout (KO) iPSCs remained unchanged compared to isogenic control iPSCs. Following small molecule-mediated differentiation into cortical glutamatergic neurons however, we detected a significant delay in transition from proliferating radial glia cells/NPCs to postmitotic neurons in CUL3 KO cultures. Notably, direct neural conversion of CUL3 KO iPSCs by lentiviral expression of Neurogenin-2 massively attenuated the neurodevelopmental delay. However, both optogenetic and electrical stimulation of induced neurons revealed decreased excitability in Cullin-3 deficient cultures, while basal synaptic transmission remained unchanged. Analysis of target gene expression pointed to alterations in FGF signaling in CUL3 KO NPCs, which is required for NPC proliferation and self-renewal, while RhoA and Notch signaling appeared unaffected. Our data provide first evidence for a major role of Cullin-3 in neuronal differentiation, and for neurodevelopmental deficits underlying neuropsychiatric disorders associated with CUL3 mutations.

57

**Keywords:** Neuropsychiatric disorders, CUL3, CRISPR/Cas9 nickase, induced pluripotent stem cells, human glutamatergic neurons, direct neuronal conversion

**60 INTRODUCTION**

61

62 Schizophrenia (SZ) is a severe neuropsychiatric disorder that affects about 21 million people  
63 worldwide and has a prevalence of approximately 1% (Lewis DA and Gonzalez-Burgos G,  
64 2006; Millan MJ et al., 2016). SZ patients exhibit both positive symptoms (e.g. hallucinations,  
65 disorganized thought and speech), and negative symptoms, (e.g. cognitive impairments, social  
66 withdrawal) (Lewis DA and Gonzalez-Burgos G, 2006; Millan MJ et al., 2016). Since current  
67 medications mainly alleviate positive symptoms, there is a high unmet medical need for novel  
68 therapies targeting negative symptoms (reviewed in (Brennand KJ et al., 2011)).  
69 Environmental factors (e.g. stress in early life) increase the risk for SZ, but there is also a  
70 strong genetic component with a heritability of approximately 80% (Bahari-Javan S et al., 2017;  
71 Sullivan PF et al., 2003; Walsh T et al., 2008).

72 In 2014, a landmark genome-wide association study (GWAS) reported 108 schizophrenia-  
73 associated genomic loci representing low risk, common variants (Schizophrenia Working  
74 Group of the Psychiatric Genomics C, 2014). In this study, the CUL3 gene, which encodes the  
75 E3 ubiquitin ligase Cullin-3, was assigned to a non-coding risk locus by genomic proximity. In  
76 a more recent GWAS of schizophrenia, CUL3 was functionally annotated to non-coding  
77 genetic risk variants by chromatin conformation capture using both human brain tissue and  
78 iPSC-derived cortical neurons (Li M et al., 2018; Rajarajan P et al., 2018). Whether these non-  
79 coding risk variants increase or decrease CUL3 gene expression remains to be tested. The  
80 CUL3 gene is also affected by rare, high risk, *de novo* mutations in protein coding regions in  
81 patients diagnosed with SZ or autism spectrum disorder (ASD) (Lin GN et al., 2015). Moreover,  
82 CUL3 is listed as one of 23 high confidence risk genes for ASD in the SFARI Gene database  
83 ([gene.safari.org/database](http://gene.safari.org/database)). The E3 ubiquitin ligase Cullin-3 targets protein substrates for  
84 proteasomal degradation (reviewed in (Hershko A and Ciechanover A, 1998)). Cullin-3 binds  
85 to specific adaptor proteins that are important for recognition and ubiquitylation of protein  
86 substrates. Notably, protein-truncating, *de novo* mutations in CUL3 were detected in ASD  
87 patients, which disrupt Cullin-3 interaction with its adaptor, potassium channel tetramerization  
88 domain containing 13 protein (KCTD13) (Lin GN et al., 2015).

89 During the last decade, numerous iPSC lines were generated from patients diagnosed with  
90 various neuropsychiatric diseases. Differentiation of human iPSCs into forebrain neurons and  
91 subsequent structural/functional analyses contributed to a better understanding of the  
92 neurodevelopmental pathomechanisms that increase the risk for neuropsychiatric disorders  
93 (Brennand KJ et al., 2011; Marchetto MC et al., 2010; Murai K et al., 2016; Pasca SP et al.,  
94 2011; Sheridan SD et al., 2011). Several points are speaking in favor of CUL3 disease



95 modeling in iPSC-derived cortical glutamatergic neurons: (i) co-expression of CUL3 and its  
96 adaptor KCTD13 is high in the mid-fetal period of the developing human cortex (Kang HJ et  
97 al., 2011; Lin GN et al., 2015), (ii) the transcriptomic profile of human iPSC-derived neurons  
98 correlates best with that of human mid-fetal cortical neurons (Brennand K et al., 2015; van de  
99 Leemput J et al., 2014), and (iii) gene co-expression network analysis based on nine high  
100 confidence ASD risk genes including CUL3 showed convergence in mid-fetal cortical  
101 glutamatergic neurons (Willsey AJ et al., 2013). In the present study, we used CRISPR/Cas9  
102 nickase to generate CUL3 knockout (KO) human iPSC lines and isogenic controls. This  
103 approach reduces off-target DNA cleavage observed with Cas9 nuclease (Ran FA et al., 2013),  
104 and minimizes the high variability observed with case/control iPSC lines carrying a different  
105 genetic background (Kyttala A et al., 2016). We differentiated the heterozygous CUL3 KO iPSC  
106 lines and the isogenic control iPSC lines into neural progenitor cells (NPCs) and cortical  
107 glutamatergic neurons using two protocols that others have employed to functionally assign  
108 non-coding SZ risk loci to causal genes by open chromatin profiling and chromatin interaction  
109 assays (Forrest MP et al., 2017; Rajarajan P et al., 2018). Small molecule-mediated neuronal  
110 differentiation revealed a massive delay in transition from proliferating radial glia cells/NPCs to  
111 postmitotic neurons in CUL3 KO cultures. This neurodevelopmental delay was not detectable  
112 by direct neuronal conversion of CUL3 KO iPSCs, however, induced Cullin-3 deficient neurons  
113 showed decreased excitability. Taken together, our study provides first evidence for a role of  
114 Cullin-3 ubiquitin ligase in human neurodevelopment and for potential neurodevelopmental  
115 deficits in psychiatric patients carrying CUL3 loss-of-function mutations.

116

117

## 118 **EXPERIMENTAL PROCEDURES**

119

### 120 **Culture of human induced pluripotent stem cells**

121 The quality-controlled (Sendai virus clearance, pluripotency, normal karyotype) human iPSC  
122 line SB Ad3 clone 4 (reprogrammed from skin fibroblasts of a 31 years old, healthy donor) was  
123 obtained from the StemBanc consortium (Kizner V et al., 2019; Morrison M et al., 2015). All  
124 iPSC lines were maintained under feeder-free conditions in Essential 8 medium (Gibco, Big  
125 Cabin, OK, USA) supplemented with 1:100 Antibiotic-Antimycotic (Life Technologies, Carlsbad,  
126 CA, USA). Cells were seeded on 6-well tissue culture plates (Sarstedt, Nümbrecht, Germany)  
127 coated with Matrigel basement membrane matrix (Corning, Corning, NY, USA). Matrigel was  
128 diluted 1:10 in DMEM/F12 and Glutamax (Gibco, Big Cabin, OK, USA). Cells were split before  
129 reaching 100% confluence using 0.02% EDTA (Sigma-Aldrich, St. Louis, MO, USA) and were  
130 replated in E8 medium supplemented with 10  $\mu$ M ROCK inhibitor Y27632 (Tocris, Bristol,

131 United Kingdom). Cells were cultured at 37°C and 5% CO<sub>2</sub>. All iPSC lines and iPSC-derived  
132 cells were negatively tested for mycoplasma using MycoAlert™ PLUS Mycoplasma Detection  
133 Kit (Lonza, Basel, Switzerland) according to the manufacturer's protocol.

134

### 135 **Genome editing using CRISPR/Cas9 D10A nickase**

136 The human iPSC line SB Ad3 clone 4 (abbreviated CB4) (Morrison M et al., 2015) was used  
137 for CUL3 gene knockout by Cas9 D10A nickase and two guide RNAs (gRNAs). The gRNAs  
138 were identified using the Sanger Institute CRISPR webtool  
139 ([http://www.sanger.ac.uk/htgt/wge/find\\_crisprs](http://www.sanger.ac.uk/htgt/wge/find_crisprs)) and chosen on the basis of having the lowest  
140 combined off-targeting score whilst targeting as many of the known and predicted transcripts  
141 as possible. Since there exists no off target pairing of these gRNAs closer than 1kb to one  
142 another, we consider the possibility of off-target DNA cleavage to be negligible. Both gRNAs  
143 target exon 5 of the CUL3 gene. The antisense guide 5'-GACCTAAAATCATTAACATC-3' was  
144 cloned into the spCas9 D10A nickase expressing vector pX335 and the sense guide 5'-  
145 GAGTCTATGAAGAAGATTTTG-3' into the puromycin selectable plasmid pBABED P U6.  
146 Human iPSCs were grown to 80% confluency and treated with 10 µM ROCK inhibitor Y27632  
147 one day prior to nucleofection. Cells were dissociated into single cells using 0.5 ml Accutase  
148 (Merck). 5 µg of each plasmid were mixed with the nucleofection solution of the Amaxa Human  
149 Stem Cell Nucleofector Starter Kit (Lonza, Basel, Switzerland). Nucleofection was performed  
150 using program B-016 of the Amaxa nucleofector device. Nucleofected iPSCs were seeded on  
151 Matrigel-coated 10 cm cell culture dishes containing E8 medium and 10 µM ROCK inhibitor  
152 Y27632. After 24 hours, medium was changed to E8 supplemented with 0.5 µg/ml puromycin  
153 (Merck, Darmstadt, Germany) for 3 days and replaced daily. Puromycin resistant single iPSC  
154 colonies were picked and expanded under iPSC maintenance conditions.

155

### 156 **T7 Endonuclease Assay**

157 Formation of insertions/deletions following Cas9 D10A nicking in the CUL3 exon 5 region was  
158 tested using T7 Endonuclease assay according to the protocol of the EnGen Mutation  
159 Detection Kit (New England Biolabs, Ipswich, MA, USA). DNA of iPSC clones was extracted  
160 using QuickExtract™ DNA Extraction Solution 1.0 according to the manufacturer's protocol  
161 (Epicentre, Madison, WI, USA). Genomic regions encompassing the gRNA target sites were  
162 amplified using forward primer 5'-GCTGCAGCTAAAGTGGCTTG-3' and reverse primer 5'-  
163 AGCCTGCAGATGAGACTTCG-3'. Annealing temperature was calculated using Tm calculator  
164 from New England Biolabs (<https://www.neb.com/>). PCR amplification was performed using  
165 the following cycling conditions: 1 cycle for 30 seconds at 98°C, 35 cycles for 5, 10 and 50  
166 seconds at 98°C, 65°C and 72°C respectively, followed by 1 cycle for 7 minutes at 72°C. PCR

167 products were electrophoretically separated on a 2% E-Gel Precast Agarose Gel stained with  
168 ethidium bromide (Thermo Fisher Scientific, Waltham, MA, USA) on an E-Gel iBase™ Power  
169 System device (2 min of PRE-RUN and program 1E-Gel 0.8-2%) for 26 min. Images were  
170 analyzed using the ChemiDoc gel imaging system (Bio-Rad, Hercules, CA, USA). Fragment  
171 analysis considered samples with only one full-length, non-cleaved band as negative clones,  
172 whereas more than two bands indicate insertion/deletion formation following Cas9 D10A  
173 nicking.

174

### 175 **Karyotype analysis**

176 DNA was extracted from nucleofected iPSC clones using Qiagen AllPrep DNA/RNA Micro Kits  
177 according to the manufacturer's protocol (Qiagen, Hilden, Germany). DNA samples were sent  
178 to Life & Brain Genomics (Bonn, Germany) for karyotype analysis using the Illumina BeadArray  
179 Technology (HumanOmni2.5Exome-8 BeadChip v1.3, Illumina, San Diego, CA, USA).  
180 Genotypes were analyzed using GenomeStudio V2.0.2. For copy number analysis, the CNV-  
181 Partition algorithm version 3.2 (Illumina, San Diego, CA, USA) was applied. Copy number  
182 variants were reported, if larger than 350.000 base pairs.

183

### 184 **DNA sequencing**

185 Genomic DNA encompassing the gRNA target sites was amplified using HotStart Q5  
186 Polymerase (New England Biolabs, Ipswich, MA, USA). PCR products were custom  
187 sequenced by Sequiserve (Munich, Germany).

188

### 189 **Neuronal differentiation of iPSCs using small molecules**

190 Differentiation of iPSCs into neural progenitor cells (NPCs) and cortical glutamatergic neurons  
191 was based on a well-established protocol (Shi Y et al., 2012; Shi Y et al., 2012), which others  
192 have employed to assign non-coding SZ risk variants to causal genes by open chromatin  
193 profiling (Forrest MP et al., 2017). Neural induction was initiated by incubating iPSCs (at  
194 approximately 90% confluency) for 8-12 days with Neural Induction Medium consisting of 250  
195 ml DMEM/F12 and GlutaMAX™ medium, 250 ml Neurobasal™ medium, 1.25 mg Insulin  
196 (Sigma-Aldrich, St. Louis, MO, USA), 2.5 ml Sodium Pyruvate (Sigma-Aldrich, St. Louis, MO,  
197 USA), 0.5 ml beta-mercaptoethanol, 2.5 ml Non-Essential Amino Acids Solution (100x), 1.25  
198 ml PenStrep, 2.5 ml N2 supplement (100x), 5 ml B-27™ supplement (50x, serum free), 2.5 ml  
199 L-Glutamine (all Thermo Fisher Scientific, Waltham, MA, USA), 1 µM Dorsomorphin and 10  
200 µM SB431542 (both Merck, Darmstadt, Germany). Neuroepithelial sheets were dissociated  
201 with 10 mg/ml Dispase (Thermo Fisher Scientific, Waltham, MA, USA) on day 8 and replated  
202 on laminin-coated (Sigma-Aldrich, St. Louis, MO, USA) 6 well plates. On day 13, neural rosette

203 formation was promoted by adding medium with 20 ng/ml FGF2 (R&D Systems, Minneapolis,  
204 MN, USA) for 4 days. Non-neuronal differentiation was reduced by multiple dissociation steps  
205 using 10 mg/ml Dispase. From day 17 to 25 medium was exchanged every second day. On  
206 day 25, NPCs were dissociated into single cells using Accutase (Merck, Darmstadt, Germany).  
207 For differentiation into cortical neurons, NPCs were seeded on 2x concentrated Matrigel plates.  
208 Cells were cultured in medium containing 10  $\mu$ M DAPT (STEMCELL, Vancouver, Canada), 50  
209  $\mu$ M cAMP, 20 ng/ml BDNF and 20 ng/ml GDNF (both PeproTech, Rocky Hill, NJ, USA) for four  
210 days and subsequently replated on assay plates coated with 0.07% polyethyleneimine (Sigma-  
211 Aldrich, St. Louis, MO, USA) in borate buffer and 1:100 laminin (Sigma-Aldrich, St. Louis, MO,  
212 USA). For neuronal maturation, DAPT was omitted and medium containing 50  $\mu$ M cAMP, 20  
213 ng/ml BDNF and 20 ng/ml GDNF was exchanged three times per week.

214

### 215 **Direct neuronal conversion of iPSCs using lentiviral NGN2 expression**

216 Human iPSCs were directly converted into glutamatergic cortical neurons by tetracycline-  
217 inducible expression of the neuralizing transcription factor Neurogenin-2 (NGN2) following  
218 lentiviral transduction as originally described by Zhang et al (Zhang Y et al., 2013). Lentiviral  
219 production was performed as described elsewhere (Colasante G et al., 2015). For accelerated  
220 induction of excitatory neurons, we combined direct NGN2-mediated conversion with  
221 developmental patterning, as recently reported by others (Nehme R et al., 2018; Qi Y et al.,  
222 2017). Human iPSC were patterned towards a dorsal forebrain phenotype by pharmacological  
223 inhibition of TGF-beta, BMP, and WNT signaling using SB431542 (10  $\mu$ M), LDN193189 (250  
224 nM), and XAV939 (5  $\mu$ M). To accelerate neuronal fate acquisition, we additionally inhibited  
225 FGF, Notch, and MEK signaling using SU5402 (10  $\mu$ M), DAPT (10  $\mu$ M), and PD0325901 (8  
226  $\mu$ M). Induced neurons were replated and cocultured with rat primary cortical astrocytes  
227 (Thermo Fisher Scientific, Waltham, MA, USA) on day 8 post transduction in order to promote  
228 neuronal maturation and synapse formation (Zhang Y et al., 2013).

229

### 230 **Quantitative real time PCR (qRT-PCR)**

231 Cells were lysed in RLT buffer (Qiagen, Hilden, Germany) supplemented with 1% beta-  
232 mercaptoethanol (Carl Roth, Karlsruhe, Germany). Lysates were homogenised using  
233 QIAshredder columns (Qiagen, Hilden, Germany) and total RNA was extracted using RNeasy  
234 Mini Kit (Qiagen, Hilden, Germany) as described in the manufacturer's protocol including an  
235 on-column DNase digestion step. RNA concentration and quality were analyzed using a  
236 NanoDrop 1000 device (Thermo Fisher Scientific, Waltham, MA, USA). RNA was reverse  
237 transcribed to cDNA using SuperScript VILO cDNA Synthesis Kit (Invitrogen, Carlsbad, CA,

238 USA) according to manufacturer's protocol. For PCR analysis triplicates of cDNA samples  
239 were amplified using TaqMan Gene Expression Assay (Thermo Fisher Scientific, Waltham,  
240 MA, USA and QuantiFast Probe RT-PCR MasterMix (Qiagen, Hilden, Germany). Validated  
241 primer pairs for human transcripts were acquired from Thermo Fisher Scientific (Waltham, MA,  
242 USA). The CUL3 primer pair binds on the exon 14-15 boundary. PCR data were analyzed  
243 using QuantStudio™ 6 Flex Real-Time PCR System (Applied Biosystems, Foster City, CA,  
244 USA). Samples were normalised to the housekeeping gene POLR2A and evaluated by the  
245  $\Delta\Delta C_T$  method.

246

### 247 **Immunocytochemical analysis**

248 Cells were fixed in 4% paraformaldehyde (Sigma-Aldrich, St. Louis, MO, USA) in phosphate-  
249 buffered saline (PBS) for 15 minutes at room temperature. After three washing steps, cells  
250 were permeabilized in 0.1% Triton X-100 (Sigma-Aldrich, St. Louis, MO, USA) for 15 minutes.  
251 Unspecific protein binding was blocked in 5% Normal Goat Serum (Cell Signaling Technology,  
252 Danvers, MA, USA) at room temperature for 2 hours. Primary antibodies were diluted in 10%  
253 Fetal Bovine Serum (Gibco, Big Cabin, OK, USA) and incubated over night at 4°C. Primary  
254 antibodies used for immunocytochemistry are listed in Supplementary Table 1. Alexa-  
255 conjugated secondary antibodies were diluted in 5% Fetal Bovine Serum and incubated for 2  
256 hours at room temperature, protected from light. Hoechst 33342 dye (1:2000 in PBS)  
257 (Molecular Probes, Eugene, OR, USA) was used to stain nuclei. For detection of the  
258 fluorescent signals, the Opera Phenix™ High-Content Screening System (PerkinElmer,  
259 Waltham, MA, USA) at 20x or 63x magnification was used. Digital images were analyzed using  
260 Columbus software (Version 2.7.0.130974, PerkinElmer, Waltham, MA, USA) as described in  
261 detail elsewhere (Kizner V et al., 2019). Dead cells showing condensed/fragmented nuclei  
262 were excluded from analysis. The ratio of immunofluorescent cells to viable cells (Hoechst-  
263 positive, non-condensed/non-fragmented nuclei) was calculated to evaluate the percentage of  
264 immunopositive cells.

265

### 266 **Immunoblot analysis**

267 Cells were lysed in Cell Lysis Buffer (Cell Signaling Technology, Danvers, MA, USA)  
268 supplemented with 1:100 protease inhibitor cocktail and phosphatase inhibitor cocktail 2 (both  
269 Sigma). Samples were incubated on ice for 15-20 min. Subsequently, cell debris was pelleted  
270 by centrifugation at 21000xg for 10 min at 4°C, and supernatants were used for further analysis.  
271 Protein concentrations were determined using BioRad Assay Dye Reagent and a microplate  
272 reader Wallac Victor (Perkin Elmer). Briefly, 10 µl of BSA protein standards and 10 µl protein  
273 samples (diluted 1:10 in ddH<sub>2</sub>O) were added to a 96-well plate. 200 µl BioRad Assay Dye

274 Reagent was added and incubated for 5 min in the dark. Plate was measured and protein  
275 concentration was calculated using Excel and GraphPad Prism. SDS gel-electrophoresis of  
276 protein lysates was performed using NuPAGE™ 4-12% Bis-Tris Protein Gels (Life  
277 Technologies, Carlsbad, CA, USA) at 200 V for 45 minutes in 3-(N-morpholino)propanesulfonic  
278 acid (MOPS) buffer (Invitrogen, Carlsbad, CA, USA). Proteins were transferred to a  
279 nitrocellulose membrane in Tris-Glycine Buffer (Bio-Rad, Hercules, CA, USA) supplemented  
280 with 20% methanol at 100 V for 90 minutes. MemCode Reversible Protein Stain (Thermo  
281 Fisher Scientific, Waltham, MA, USA) was used to assess equal protein loading. Membranes  
282 were blocked with 5% milk powder in TBS and 0.1% Tween20 (TBST) for 2 hours followed by  
283 incubation with primary antibodies at 4°C overnight. Primary antibodies are listed in  
284 Supplementary Table 1. HRP-conjugated secondary antibodies were added for 2 hours, and  
285 protein bands were visualised by enhanced chemiluminescence using Western Lightning Plus-  
286 ECL reagent (PerkinElmer, Waltham, MA, USA). Some blot membranes were stripped using  
287 Pierce Restore Western Blot Stripping Buffer (Thermo Fisher Scientific, Waltham, MA, USA)  
288 for 15 min at room temperature, washed in TBST, blocked and incubated with antibodies as  
289 described above. Blots were imaged using a ChemiDoc Imaging System (Bio-Rad, Hercules,  
290 CA, USA) and volume band intensity was quantified using ImageLab Software (Bio-Rad,  
291 Hercules, CA, USA).

292

### 293 **Modeling of protein structure**

294 Modeling of 3-dimensional protein structure was based on the amino acid sequence of Cullin-3  
295 protein available from UniProt Knowledgebase (<http://www.uniprot.org/uniprot/Q13618>),  
296 the protein structure homology-modeling software from SWISS-MODEL  
297 (<https://swissmodel.expasy.org/interactive>) (Waterhouse A et al., 2018) and the molecular  
298 visualisation software PyMOL (The PyMOL Molecular Graphics System, Version 2.0  
299 Schrödinger, LLC).

300

### 301 **EdU labeling of proliferating cells**

302 Click-iT EdU Imaging Kit including Alexa Fluor® 488, 594 and 647 Azides (Life Technologies,  
303 Carlsbad, CA, USA) was used according to the manufacturer's protocol. 20 µM EdU solution  
304 was added to proliferating iPSCs/NPCs and incubated at 37°C for 60 minutes. Cells were fixed  
305 in 4% PFA for 15 minutes at room temperature, followed by permeabilisation in 0.5% Triton X-  
306 100 for 20 minutes. Click-iT reaction cocktail was added to each well and incubated for 30  
307 minutes, protected from light. Hoechst 33342 (1:16000 in PBS) was added for nuclear DNA  
308 counterstaining. Detection of EdU positive cells was performed using Opera Phenix™ High-  
309 Content Screening System (PerkinElmer, Waltham, MA, USA) (20x water objective and

310 channels Alexa488, Alexa594, Alexa647 and DAPI). Images were analyzed using Columbus  
311 software and the ratios of EdU-positive proliferating cells to Hoechst-positive total cells were  
312 calculated.

313

### 314 **PCR Array analyses**

315 To analyze expression of genes regulating human neurogenesis, RT<sup>2</sup> Profiler™ PCR Arrays  
316 Human Neurogenesis (Qiagen, Hilden, Germany, Format A) were used as described in the  
317 PCR array handbook (<http://www.sabiosciences.com/Manual/1070190.pdf>). RNA was  
318 extracted from NPC lysates using RNeasy Mini Kits (Qiagen, Hilden, Germany). Reverse  
319 transcription to cDNA was performed using RT<sup>2</sup> First Strand Kit (Qiagen, Hilden, Germany). A  
320 genomic DNA elimination mix was added to 500 ng RNA and incubated for 5 minutes at 42°C  
321 followed by 1 minute on ice. Reverse-transcription mix was then added to the genomic DNA  
322 elimination mix and incubated for another 15 minutes at 42°C. Reaction was stopped by  
323 incubation at 95°C for 5 minutes. 2xRT<sup>2</sup> SYBR Green Mastermix and RNase-free-water were  
324 added to the cDNA. Real-time PCR was performed using QuantStudio 6k Flex (Applied  
325 Biosystems, Foster City, CA, USA). Cycling conditions were as follows: 1 cycle for 10 minutes  
326 at 95°C, and 40 cycles with 15 seconds (95°C) and 1 minute (60°C). Baseline settings were  
327 calculated automatically, whereas the threshold ( $\Delta R_n$  vs cycle) was manually set to 0.05. Gene  
328 expression was analyzed using the  $\Delta\Delta C_T$ -method and the online Qiagen software tool  
329 ([www.sabiosciences.com/pcrdataanalysis.php](http://www.sabiosciences.com/pcrdataanalysis.php)). The  $C_T$  cut-off was set to 30. Genes with a  
330 fold-regulation greater than 2 or smaller than -2 compared to the wildtype clones were  
331 considered as deregulated. P-values were calculated by comparing the three wildtype clones  
332 versus the three CUL3 knockdown clones, and p-value threshold was set to 0.1.

333 To analyze expression of human genes encoding neurotransmitter receptors/transporters,  
334 TaqMan™ Arrays Human Neurotransmitters (Applied Biosystems, Foster City, CA, USA) were  
335 used according to the manufacturer's manual ([https://assets.thermofisher.com/TFS-Assets/LSG/manuals/cms\\_053406.pdf](https://assets.thermofisher.com/TFS-Assets/LSG/manuals/cms_053406.pdf)). Sample preparations and experimental procedures  
336 were performed as described in the PCR array handbook  
337 (<http://www.sabiosciences.com/Manual/1070190.pdf>) and below. Post-mitotic neurons derived  
338 from iPSCs were lysed in RLT-buffer supplemented with 1% beta-mercaptoethanol after 16  
339 days of maturation. RNA was extracted using RNeasy Micro Kit according to the  
340 manufacturer's protocol (Qiagen, Hilden, Germany). Transcription to cDNA was performed as  
341 described in the manual of the High-Capacity cDNA Reverse Transcription Kit (Applied  
342 Biosystems, Foster City, CA, USA). TaqMan Gene Expression Master Mix (Thermo Fisher  
343 Scientific, Waltham, MA, USA) was added to the cDNA samples. Real-time PCR was  
344 performed using QuantStudio 6k Flex (Applied Biosystems, Foster City, CA, USA). Cycling  
345

346 conditions and instrument settings are described in the Neurogenesis PCR Array chapter  
347 above. For data evaluation,  $C_T$ -values were exported to Excel and analyzed using the  $\Delta\Delta C_T$ -  
348 method. The  $C_T$  cut-off was set to 30. Genes with a fold-regulation greater than 2 or smaller  
349 than -2 compared to the wildtype clones were considered as deregulated. P-values were  
350 calculated by comparing the three wildtype clones versus the three knockdown clones and p-  
351 value threshold was set to 0.05.

352

### 353 **Multi-electrode array recordings and optogenetic stimulation**

354 Multi-electrode array (MEA) plates (24-well, Multi Channel Systems MCS, Reutlingen,  
355 Germany) were coated by adding 100  $\mu$ l polyethylenimine solution (0.07%) per well and  
356 incubating for 1h at 37°C. Plates were rinsed twice with PBS and water and dried overnight.  
357 On the following day, neurons were dot-seeded on the electrode area at a density of 120,000  
358 cells per well in 10  $\mu$ l medium containing 80  $\mu$ g/ml laminin. After 1h incubation at 37°C, medium  
359 volume was increased to 500  $\mu$ l. A 50% medium exchange was performed every 2-3 days.  
360 Spontaneous extracellular field potentials were recorded at 37°C under a 5% CO<sub>2</sub> atmosphere  
361 using the Multiwell-MEA system and Multiwell Screen software (Multi Channel Systems MCS,  
362 Reutlingen, Germany). After an equilibration period of 5 min, recordings were performed for  
363 10 min at a sampling rate of 20 kHz. A 10 Hz to 2.5 kHz bandwidth filter was applied. Data  
364 analysis was performed using Multiwell Analyzer software (Multi Channel Systems MCS,  
365 Reutlingen, Germany). Spikes were counted, if the recorded signal exceeded a threshold of 5  
366 times the standard deviation of the baseline noise level. Electrodes were considered active, if  
367 the spike rate exceeded 0.1 Hz. A burst was defined as a series of at least 7 consecutive  
368 spikes with a maximum inter-spike interval of 50 ms. Network bursts were counted, if a  
369 minimum of 8 out of 12 electrodes per well recorded simultaneous burst-firing. Multiparametric  
370 analysis of spikes, bursts and network bursts was performed using Microsoft Excel (Microsoft  
371 Corporation, Redmond, WA, USA) and GraphPad Prism 8 (GraphPad Software, San Diego,  
372 CA, USA). For artifact-free, precise stimulation, iPSCs were transduced both with a lentiviral  
373 vector encoding channelrhodopsin-2 (ChR2), a light-gated cation channel (Nagel, PNAS,  
374 2003), tagged with a fluorescent EYFP reporter and with lentiviral NGN2. On day 34 of  
375 neuronal maturation, brief (50 ms) blue light pulses (470 nm) were applied to ChR2 expressing  
376 neurons by a 3x24 light emitting diodes (LEDs) carrying device (LED stimulator MW24-opto-  
377 stim, Multi Channel Systems MCS, Reutlingen, Germany) that was positioned onto the MEA  
378 plate. Light intensity was modulated by applying pulses at controlled currents ranging from 2  
379 mA to 5 mA (Multiwell-Screen software, Multi Channel Systems MCS, Reutlingen, Germany).

380

### 381 **Calcium imaging**



382 Calcium imaging was performed using a fluorometric imaging plate reader (FLIPR Tetra,  
383 Molecular Devices, San Jose, CA, USA). Neurons were seeded into 384-well plates coated  
384 with poly-L-lysine, laminin and fibronectin (all Sigma-Aldrich, St. Louis, MO, USA) at a density  
385 of 5000 cells per well on day 8 post transduction. After three weeks of maturation, the plates  
386 were carefully washed with Ringer buffer consisting of 130 mM NaCl, 5 mM KCl, 1 mM CaCl<sub>2</sub>,  
387 1 mM MgCl<sub>2</sub>, 2 mM KH<sub>2</sub>PO<sub>4</sub>, 20 mM HEPES and 5 mM glucose at pH 7.4. Measurements of  
388 intracellular calcium were performed after 1 hour incubation with Calcium 4 assay reagent  
389 (Molecular Devices, San Jose, CA, USA). Briefly, 1 minute baseline recording was followed by  
390 stepwise electrical stimulation at a constant voltage of 12V with 5 seconds stimulation each at  
391 2, 5, 10, 20 and 50 Hz in 2-minute intervals. Neuronal excitability was calculated by subtracting  
392 the baseline signal from maximal relative light units in response to electrical stimulation and  
393 normalizing the resulting value to the baseline.

394

### 395 **Statistical analysis**

396 Biological assays were performed using the wildtype parental iPSC line and two heterozygous  
397 CUL3 knockout iPSC lines showing different deletions. In addition, two iPSC lines, which went  
398 through nucleofection and selection, but did not show genomic modifications, were included  
399 as controls. No statistical methods were used to predetermine sample size. However, the  
400 sample sizes in our study are similar to those reported in previous publications (Brennan KJ  
401 et al., 2011; Kizner V et al., 2019; Pak C et al., 2015) that showed significance. The sample  
402 sizes and the description of the sample collection are reported in the figure legends. For MEA  
403 recordings, FLIPR-based calcium imaging, and high-content microscopic screening, the cells  
404 were randomly assigned to the cell culture plates. For subsequent data acquisition,  
405 investigators were blinded with regard to the group category.

406 Graph Pad Prism version 8 (GraphPad Software, San Diego, USA) was used for all statistical  
407 analyses and graphing. Inferential statistical strategies of continuous variables are based on  
408 parametric one-factorial or two-factorial linear models (Welch's ANOVA or two-way ANOVA)  
409 followed by pairwise comparisons using a t-test modification according to Welch to account for  
410 unequal standard deviations in both groups. Discrete count data are analyzed using a non-  
411 parametric, rank-based Kruskal-Wallis test followed by pairwise Mann-Whitney U tests.

412 The significance level is set to 5% per hypothesis. P values in the figures are presented as  
413 follows: \* $p \leq 0.05$ , \*\* $p \leq 0.01$ , \*\*\* $p \leq 0.001$ , \*\*\*\* $p \leq 0.0001$ . Data are shown as mean  $\pm$  standard  
414 error of the mean (SEM). In box-and whiskers plots the box depicts the median and the 25th  
415 and 75th quartiles, and the whiskers show the 5th and 95th percentile. Additional information  
416 on statistical analysis (e.g. degrees of freedom, statistic's values, exact p-values) is given in  
417 Supplementary Table S2.

418

419

420 **RESULTS**

421

422 **Generation of CUL3 knockout iPSC lines and isogenic controls**

423 CUL3 is a high risk gene for neuropsychiatric disorders (Codina-Sola M et al., 2015;  
424 Schizophrenia Working Group of the Psychiatric Genomics C, 2014), but little is known about  
425 its function in human neurons. To get a better insight into the role of CUL3 in human  
426 neurodevelopment, we investigated the consequences of CUL3 knockout (KO) in human iPSC  
427 and iPSC-derived cortical neurons. We used CRISPR/Cas9-mediated genome modification,  
428 which enables the generation of isogenic iPSC lines, thereby reducing genetic background  
429 heterogeneity and experimental variability (Jinek M et al., 2012; Kim HS et al., 2014). We  
430 selected the human iPSC line SB Ad3 clone 4 (abbreviated CB4), which has been generated  
431 and validated by the StemBancc consortium (Morrison M et al., 2015). Human iPSCs were  
432 nucleofected with plasmid vectors encoding Cas9 D10A nickase (Cas9n) and antisense  
433 gRNAs targeting exon 5 of the CUL3 gene. The Cas9n double-nicking approach was chosen,  
434 in order to increase target specificity and reduce off-target effects as shown by others (Ran FA  
435 et al., 2013). Guide RNA off-target analysis revealed 10 potentials off-targets showing  $\geq 3$   
436 mismatches and a low score. Importantly, there is no off-target pairing of these gRNAs closer  
437 than 1 kb to one another, such that the possibility of off-target DNA cleavage is considered to  
438 be negligible.

439 Following nucleofection and puromycin selection, iPSC clones carrying CRISPR/Cas9n-  
440 mediated insertions/deletions were identified by T7 endonuclease assay (Fig. 1A). Only iPSC  
441 clones showing a normal karyotype were included in subsequent analyses. By genomic DNA  
442 sequencing we detected a 3 base pair (bp) deletion in the heterozygous CUL3 KO iPSC clone  
443 6, and a 17 bp deletion in the heterozygous CUL3 KO iPSC clone 19 (Fig. 1C). According to  
444 UniProt Knowledgebase, either amino acid Glu202 or Glu203 of human Cullin-3 protein  
445 (Q13618) was deleted in clone 6. The 17 bp frameshift deletion in clone 19 is predicted to lead  
446 to a premature stop codon following amino acid 199 (p.Phe199X), which may result in  
447 nonsense-mediated mRNA decay (Chang YF et al., 2007) of the mutant transcript, or  
448 translation of a truncated, likely inactive Cullin-3 protein fragment from the mutant allele. Cullin-  
449 3 has an N-terminal domain that comprises three repeats with five alpha-helix bundles each  
450 (Petroski MD and Deshaies RJ, 2005). Our modeling of the 3-dimensional protein structure of  
451 Cullin-3 using SWISS-MODEL and PyMOL software revealed that amino acids 202/203 are  
452 located in alpha-helix C of repeat 2 of the Cullin-repeat motif (Petroski MD and Deshaies RJ,

453 2005; Zheng N et al., 2002). Uniprot Knowledgebase also showed that amino acids Glu202  
454 and Glu203 are highly conserved between species. Moreover, a potentially deleterious, in-  
455 frame deletion of Glu203 (variant 2:225378283 p.Glu203del) in human Cullin-3 has been  
456 reported by the Exome Aggregation Consortium (Lek M et al., 2016). Similar to CUL3 gene  
457 targeting in mice (Singer JD et al., 1999), we did not detect a homozygous CUL3 KO clone. In  
458 addition to the wildtype parental iPSC line CB4, two iPSC clones (clone 2 and clone 13), which  
459 went through CRISPR/Cas9 nucleofection, but did not show insertions/deletions, were  
460 included as controls in subsequent analyses.

461 Quantitative real-time polymerase chain reaction (qRT-PCR) confirmed an approximately 50%  
462 decrease in CUL3 mRNA expression in heterozygous CUL3 KO iPSC clones (Fig. 1B).  
463 Consistently, Cullin-3 protein levels were significantly reduced in heterozygous CUL3 KO  
464 iPSCs, as shown by immunoblot analyses using both a monoclonal anti-Cullin-3 antibody  
465 against the N-terminus of human Cullin-3, and a polyclonal anti-Cullin-3 antibody against the  
466 C-terminus (Fig. 2). In protein lysates from heterozygous CUL3 KO clone 19, a truncated  
467 Cullin-3 protein fragment was not detected, and the Cullin-3 protein band was shifted towards  
468 a slightly higher molecular weight (Fig. 2A). In addition, by total protein staining of the blots we  
469 did not detect protein bands with increased intensity in the heterozygous CUL3 KO iPSC lines  
470 (Fig. 2A). This suggests that a heterozygous loss of CUL3 has a moderate effect on protein  
471 ubiquitination/degradation, or that Cullin-3 preferentially acts on low abundance proteins that  
472 are not detectable by our protein stain.

473

#### 474 **CUL3 deficiency does not affect stemness of human iPSCs**

475 Since CUL3 is highly expressed in human iPSCs (Fig. 1B) (van de Leemput J et al., 2014), we  
476 investigated its potential role in stemness by immunostaining for marker proteins. Expression  
477 of the cell surface protein Tra1-60 and the nuclear protein Oct-4 was assessed in iPSC cultures  
478 by high-content digital image analysis (Fig. 3). More than 98% of the iPSCs were  
479 immunopositive for Oct-4 both in heterozygous CUL3 KO cultures (clones 6 and 19) and in  
480 isogenic controls (clones CB4, 2, and 13) (n = 11 wells per clone). Percentage of Tra1-60  
481 immunopositive cells did not significantly differ between the genotypes as well. Furthermore,  
482 high-content image analysis of the percentage of viable iPSC cells showing Hoechst-positive,  
483 non-condensed/non-fragmented nuclei did not show significant differences between the  
484 genotypes, which indicates that cell viability and proliferation are unaltered.

485

#### 486 **NPCs differentiated from heterozygous CUL3 knockout iPSCs exhibit a moderate** 487 **increase in cell proliferation**

488 CUL3 deficiency in mouse embryonic fibroblasts resulted in an increased percentage of cells  
489 in S phase of the cell cycle (McEvoy JD et al., 2007). To examine the effect of CUL3 deficiency  
490 on proliferation of human iPSCs and NPCs, we analyzed incorporation of 5-ethynyl-2-  
491 deoxyuridine (EdU) during DNA replication by high-content image analysis of cell cultures. The  
492 percentage of iPSCs showing EdU-positive nuclei showed a trend ( $p > 0.05$ ) towards increased  
493 proliferation in the two heterozygous CUL3 KO clones compared to isogenic wildtype control  
494 clones (Fig. 4B). The percentage of NPCs showing EdU-positive nuclei was moderately, but  
495 significantly increased in the two heterozygous CUL3 KO clones compared to isogenic wildtype  
496 controls (Fig. 4B). Similar iPSC cell proliferation and iPSC cell density between the genotypes  
497 make an indirect effect on neural cell-fate commitment (Chambers SM et al., 2009) unlikely.  
498

499 **PCR array analyses reveal increased mRNA expression of PAX6 in heterozygous CUL3**  
500 **KO NPC cultures and altered mRNA expression of neurotransmitter**  
501 **receptor/transporters in CUL3 KO neurons**

502 To assess a potential function of Cullin-3 in human neurodevelopment more broadly, we  
503 analyzed mRNA expression of 84 genes regulating neurodevelopment using 96-well RT<sup>2</sup>  
504 Profiler PCR Arrays Human Neurogenesis. RNA extracts from the five NPC clones were  
505 analyzed using one PCR array each as described in detail in the Experimental Procedures  
506 section. Data analysis using the manufacturer's online software showed a 5-fold and 4-fold  
507 increase in PAX6 mRNA levels in heterozygous CUL3 KO clones 6 and 19, respectively (Fig.  
508 5A), whereas expression of TENM1 mRNA decreased 2-fold. All other arrayed genes were not  
509 differentially expressed at a  $C_T$  cut-off of 35 and a p-value threshold of 0.1. Since PCR array  
510 analysis generated only a single data point per transcript, we subsequently analyzed PAX6  
511 mRNA expression by qRT-PCR in order to demonstrate statistical significance. Consistent with  
512 data from PCR array analysis, PAX6 mRNA levels significantly increased approximately 3-fold  
513 in heterozygous CUL3 KO clones 6 and 9 compared to isogenic wildtype clones (Fig. 5A).  
514 Immunostaining of NPC cultures and digital image analysis also showed increased numbers  
515 of strongly Pax-6 immunofluorescent nuclei in heterozygous CUL3 KO clones, whereas Nestin  
516 immunofluorescence was unchanged (Fig. 5C).

517 Next, we analyzed expression of 92 neurotransmitter receptors/transporters in iPSC-derived  
518 cortical neurons after 2 weeks of differentiation/maturation using 96-well qPCR Arrays Human  
519 Neurotransmitter (as described in detail in the Experimental Procedures section). Data  
520 analysis using the manufacturer's online software revealed a significant (p-value threshold  
521 0.05) decrease in mRNA levels of the gamma-aminobutyric acid type A receptor gamma 1  
522 subunit (GABRG1), and the serotonin receptor 5-hydroxytryptamine receptor 2A (HTR2A) in  
523 heterozygous CUL3 KO iPSC-derived neurons. Notably, mRNA expression of the glutamate

524 transporter solute carrier family 1 member 3 (SLC1A3/EAAT1/GLAST1) showed a significant  
525 increase in CUL3 KO neuron cultures, which we confirmed by qRT-PCR (Fig. 5B). In the adult  
526 human brain, SLC1A3 is preferentially expressed in mature astrocytes (Hertz L and Zielke HR,  
527 2004), whereas in the developing human neocortex, SLC1A3 is expressed in proliferating  
528 radial glia cells (RGCs) and NPCs (Polioudakis D et al., 2019; Zhong S et al., 2018). Since  
529 GFAP-immunopositive astrocytes become detectable only after about 6 weeks of small  
530 molecule differentiation of human iPSCs *in vitro* ((Shi Y et al., 2012) and present study), higher  
531 levels of the RGC/NPC marker PAX6 and SLC1A3 versus lower levels of neurotransmitter  
532 receptors may indicate a delay in transition from proliferating RGCs/NPCs to postmitotic  
533 neurons in CUL3 KO cultures. Higher PAX6 mRNA expression in CUL3 KO NPCs might also  
534 indicate an enhanced pallial fate in mutant NPCs. However, this seems unlikely, since mRNA  
535 levels of the pallial marker gene LHX2 (96.1%  $\pm$  4.8%) and the subpallial marker gene DLX1  
536 (107.3%  $\pm$  10.4%) were not significantly altered in heterozygous CUL3 KO NPC cultures  
537 compared to isogenic controls.

538

539 **CUL3 KO neuron cultures exhibit a decrease in spontaneous neuronal network activity**  
540 **and an appearance of neural rosettes following small molecule-mediated differentiation**  
541 **from iPSC**

542 To test neuronal function, we dot-seeded iPSC-derived immature neurons onto 24-well glass-  
543 bottom, multi-electrode array (MEA) plates containing 12 electrodes per well. We recorded  
544 spontaneous electrical activity starting at day-in-vitro (div) 12 after seeding onto MEA plates,  
545 when action potential firing becomes detectable (Shi Y et al., 2012). At div 12 spike rate did  
546 not significantly differ between heterozygous CUL3 KO neuron cultures and isogenic wildtype  
547 controls (Fig. 6A). At div 23 spike rate in wildtype neuron cultures showed a trend towards an  
548 increase. Since neuronal differentiation/maturation using small molecules follows a more  
549 protracted time-course (Shi Y et al., 2012), this increase might become significant only at later  
550 time-points. More importantly, between div 19 and div 23 after seeding, we detected a massive  
551 decline in neuronal activity in the heterozygous CUL3 KO cultures. Bright-field microscopy of  
552 the glass-bottom MEA plates revealed the presence of numerous, radial-symmetric neural  
553 rosettes in CUL3 KO neuron cultures (inset Fig. 6A), which were not visible in isogenic controls.  
554 It may be hypothesized that these proliferating RGCs/NPCs overgrow the neuron cultures over  
555 time, and cause a decline in MEA signals by blocking contact to electrodes and/or by  
556 competing with neurons for essential medium nutrients.

557 To confirm appearance of neural rosettes composed of RGCs/NPCs during maturation of  
558 CUL3 KO iPSC-derived neurons, we performed small molecule-mediated neuronal  
559 differentiation of our iPSC lines on 96-well plates. Following immunostaining for the NPC

560 marker Pax-6 and the neuronal marker Map-2 at div 23 after replating, we detected numerous  
561 Pax-6 immunopositive RGCs/NPCs forming neural rosettes in the heterozygous CUL3 KO  
562 cultures, whereas only Map-2 positive neurons were visible in all isogenic control cultures, as  
563 expected (Fig. 7A, B). Image analysis revealed a significantly higher density of neural rosettes  
564 in cultures from heterozygous CUL3 KO clones 6 and 19 compared to isogenic wildtypes (Fig.  
565 8).

566 Cortical neurons differentiated from WT and CUL3 KO iPSC were also double immunostained  
567 for Map-2, and for vesicular glutamate transporter (vGlut-1), a marker for glutamatergic  
568 neurons. Consistent with published data (Shi Y et al., 2012), 88% – 93% of the Map-2 stained  
569 neurons were vGlut-1 positive glutamatergic neurons. High content image analysis did not  
570 detect significant differences between the genotypes. Finally, we analyzed the number of  
571 synaptic puncta labeled by the presynaptic marker, Synapsin 1/2 (Syn-1/2), and the  
572 postsynaptic marker, postsynaptic density protein 95 (Psd-95), which localize close to Map-2  
573 positive dendrites. High content image analysis revealed a significant reduction in Syn-1/2  
574 positive, presynaptic puncta per micrometer dendrite in cultures from heterozygous CUL3 KO  
575 clones 6 and 19 compared to isogenic wildtypes. (Fig. 9).

576

### 577 **Heterozygous CUL3 KO neurons show decreased excitability following direct neuronal** 578 **conversion from iPSCs**

579 Several studies have demonstrated that lentiviral expression of the transcription factor  
580 Neurogenin-2 (NGN2) directly converts human iPSCs into a homogenous population of  
581 electrically-active, cortical glutamatergic neurons within 3 weeks (Nehme R et al., 2018; Zhang  
582 Y et al., 2013). NGN2-mediated direct neuronal conversion has already been used to analyze  
583 iPSC-models of various neuropsychiatric disorders (Pak C et al., 2015; Schafer ST et al., 2019;  
584 Zhang Y et al., 2013), and may be particularly useful for high throughput screening (Wang C  
585 et al., 2017). Moreover, CUL3 has been functionally annotated to non-coding, genetic risk  
586 variants for SZ by chromatin conformation capture assays using NGN2-induced neurons  
587 (Rajarajan P et al., 2018). Therefore, we transduced the heterozygous CUL3 KO iPSC lines  
588 and the isogenic control lines with a lentivirus encoding NGN2 in a second set of experiments.  
589 Eight days after lentivirus transduction, cells were dot-seeded onto 24-well glass-bottom, MEA  
590 plates. We started recording spontaneous electrical activity at div 14 after dot-seeding, when  
591 spontaneous firing becomes detectable in NGN2-induced neurons (Nehme R et al., 2018;  
592 Zhang Y et al., 2013). Spike rate steadily increased both in heterozygous CUL3 KO neuron  
593 cultures and in isogenic wildtype control cultures following direct neuronal conversion (Fig. 6B).  
594 By multi-parametric analysis of spontaneous spikes, bursts, and network bursts, we could not  
595 detect significant differences in NGN2-induced CUL3 KO versus WT neuron cultures (Fig. 6C).

596 By bright-field microscopy of the glass-bottom MEA plates, neural rosettes were not visible in  
597 CUL3 KO cultures and in controls. In parallel, iPSC lines were directly converted into  
598 glutamatergic neurons on 96-well cell culture plates. Following immunostaining for the  
599 RGC/NPC marker Pax-6 and the neuronal marker Map-2 at div 27, only Map-2 positive  
600 neurons were detectable both in heterozygous CUL3 KO cultures and in isogenic wildtype  
601 controls (Fig. 7C, D).

602 By qRT-PCR we could detect only negligible levels of SLC1A3 mRNA expression (mean  $C_T >$   
603 35.0) in cortical neurons following NGN2-mediated direct neuronal conversion from iPSCs,  
604 which is consistent with RNA-sequencing data published by others (Tian R et al., 2019), and  
605 confirms that RGCs/NPCs are absent (Zhang Y et al., 2013). However, we detected a robust  
606 expression of CUL3 transcripts in induced wildtype neurons, which significantly decreased by  
607 approximately 50% in induced CUL3 KO neurons.

608 To analyze evoked neuronal excitability, we transduced our iPSC lines with lentiviral NGN2  
609 and a lentiviral vector encoding channelrhodopsin-2 (ChR2), which allows artifact-free,  
610 optogenetic stimulation of induced neurons on MEA plates (Clements IP et al., 2016).  
611 Exposure of ChR2 expressing neurons on MEA plates to ten brief blue light pulses (50 ms,  
612 470 nm) elicited time-locked spikes, as shown by the raster plots in Fig. 10A. As expected,  
613 exposure of transduced neurons to red light (50 ms, 590 nm) or light exposure of non-  
614 transduced neurons did not elicit any neuronal response (not shown). More importantly, the  
615 increase in spike rate following optogenetic stimulation at increasing light intensity was  
616 significantly smaller in heterozygous CUL3 KO neuron cultures compared to isogenic WT  
617 control cultures (Fig. 10B). Furthermore, at the highest light intensity, evoked activity declined  
618 in CUL3 KO cultures after 5 light pulses (Fig. 10A). Electrical stimulation and calcium imaging  
619 on a fluorometric imaging plate reader (FLIPR Tetra) confirmed decreased excitability of  
620 NGN2-induced CUL3 KO neurons (Fig. 10C), thus showing that hypoexcitability does not  
621 depend on the stimulation paradigm or the read-out.

622

### 623 **Analysis of RhoA, Notch, and FGF signaling in CUL3 KO NPCs**

624 Finally, we tried to identify the protein substrates and signaling pathways, which may be  
625 affected by Cullin-3 deficiency, and which may underlie the maintenance of the RGC/NPC  
626 stage in heterozygous CUL3 KO cultures. In non-neuronal human HeLa cells, CUL3  
627 knockdown by small hairpin RNA led to an impaired ubiquitination and degradation of the small  
628 GTPase RhoA (Chen Y et al., 2009). Moreover, network analysis implicated a Cullin-3/RhoA  
629 pathway in human brain development and psychiatric diseases (Lin GN et al., 2015). By  
630 immunoblot analysis we detected similar levels of RhoA protein in heterozygous CUL3 KO

631 iPSCs/NPCs and isogenic controls (Fig. 11A), speaking against a major contribution of altered  
632 RhoA signaling in our iPSC model.

633 During mammalian brain development, Notch receptor signaling is required to maintain NPCs  
634 in an undifferentiated, self-renewing state. Following ligand binding and receptor proteolysis,  
635 the Notch intracellular domain activates target genes of the HES/HEY families, which  
636 subsequently suppress the expression of proneuronal genes (reviewed in (Pierfelice T et al.,  
637 2011)). Conditional deletion of the Cullin-1 adaptor protein Fbxw7 leads to an accumulation of  
638 Notch protein and HES5/HEY1/HEY2 transcripts in the embryonic mouse brain, demonstrating  
639 that Notch signaling during mammalian neurodevelopment is controlled by Cullin ubiquitin  
640 ligases (Matsumoto A et al., 2011). By qRT-PCR we detected similar levels of HES5/HEY1  
641 mRNA in heterozygous CUL3 KO NPCs and isogenic WT controls, giving indirect evidence  
642 that the maintenance of RGCs/NPCs in CUL3 KO cultures during small molecule-mediated  
643 neuronal differentiation is not caused by enhanced Notch signaling. It should be noted, that we  
644 cultured proliferating NPCs in the absence of the Notch inhibitor DAPT (see Experimental  
645 Procedures), and thus, an effect of Cullin-3 deficiency on endogenous Notch signaling should  
646 be detectable by changes in Notch target gene expression.

647 Fibroblast growth factors (FGFs) are crucial for maintenance of NPCs in the developing  
648 forebrain (reviewed in (Guillemot F and Zimmer C, 2011; Mason I, 2007)), and recombinant  
649 FGF2 was added to our NPC cultures to promote proliferation and self-renewal. FGF signaling  
650 is regulated by ubiquitylation and targeted degradation of the activated FGF receptor by the  
651 ubiquitin ligase Cbl. Downstream MAPK signaling is particularly important for the mitogenic  
652 activity of FGFs. The MAPK cascade triggers transcriptional activation of effectors (e.g. ETV1,  
653 CREB1) and feedback inhibitors (e.g. SPRY1, IL17RD/SEF) of FGF receptor signaling  
654 (reviewed in (Guillemot F and Zimmer C, 2011; Mason I, 2007)). Interestingly, we detected  
655 significantly decreased mRNA levels of the feedback inhibitors SPRY1 and IL17RD/SEF in  
656 heterozygous CUL3 KO NPCs, while mRNA levels of the effectors remained unchanged (Fig.  
657 11B).

658  
659

## 660 **DISCUSSION**

661 Cullin-3 is an E3 ubiquitin ligase that ubiquitylates numerous protein substrates by binding to  
662 diverse adaptor proteins (reviewed in (Petroski MD and Deshaies RJ, 2005)). Cullin-3  
663 complexes catalyze both proteolytic and non-proteolytic ubiquitin signals, thereby regulating  
664 many fundamental biological processes, like cell division, embryonic development, DNA  
665 synthesis/repair, and cytoskeleton dynamics. Not surprisingly, loss-of-function mutations in  
666 CUL3 or its adaptor proteins are linked to severe human diseases, including metabolic



667 disorders, muscle/nerve degeneration, and cancer (reviewed in (Genschik P et al., 2013;  
668 Jerabkova K and Sumara I, 2018)). Moreover, the CUL3 gene is listed as one of the 23 top  
669 ranking, high confidence risk genes for autism spectrum disorder (ASD) in the SFARI Gene  
670 database (gene.safari.org/database). Rare, protein-truncating mutations in the CUL3 gene  
671 (e.g. p.Ser133X, p.Glu246X, p.Arg546X) were detected by independent sequencing studies in  
672 large cohorts of ASD families (da Silva Montenegro EM et al., 2019; Kong A et al., 2012;  
673 O'Roak BJ et al., 2012; Ruzzo EK et al., 2019). Unfortunately, clinical records of the mutation  
674 carriers were not reported. Large GWAS of schizophrenia have identified common, low risk  
675 genetic variants, most of them in intronic or intergenic regions of the human genome (Pardinas  
676 AF et al., 2018; Schizophrenia Working Group of the Psychiatric Genomics C, 2014). For  
677 functional annotation of these non-coding risk loci to causal genes, open chromatin profiling  
678 and chromosome interaction mapping were performed using both human brain tissue and  
679 iPSC-derived NPCs/neurons (Forrest MP et al., 2017; Li M et al., 2018; Rajarajan P et al.,  
680 2018). NPCs/neurons were derived from human iPSC using either small molecules or direct  
681 conversion, as in the present study. Notably, CUL3 was identified in chromosomal contacts  
682 anchored to SZ risk loci both in NPCs and in neurons (Rajarajan P et al., 2018; Song M et al.,  
683 2019), indicating that iPSC-derived human NPCs/neurons are well-suited to elucidate the  
684 (patho-)physiological function of Cullin-3. Whether these non-coding, gene-regulatory risk  
685 variants up- or down-regulate CUL3 gene expression, remains to be tested. Furthermore,  
686 analysis of gene coexpression modules identified CUL3 in a module (ME2) that is highly  
687 expressed in the prenatal human brain and enriched in RGCs/NPCs/neurons (Li M et al., 2018).  
688 These findings are consistent with prior network analyses of ASD risk genes including CUL3  
689 (Lin GN et al., 2015; Willsey AJ et al., 2013), and suggest that these risk variants for ASD/SZ  
690 may disrupt neurodevelopmental processes.

691 The function of Cullin-3 in the nervous system has been investigated mainly in non-mammalian  
692 species. In *Drosophila melanogaster*, a splicing mutation in CUL3 caused a massive defect in  
693 neurite elongation of mushroom body neurons (Zhu S et al., 2005), and a genetic screen  
694 identified a role for Cullin-3 in presynaptic homeostatic potentiation in the neuromuscular  
695 junction (Kikuma K et al., 2019). In the nematode *Caenorhabditis elegans*, both an  
696 endogenous protein-truncating mutation in the Cullin-3 adaptor protein KEL-8 and transgenic  
697 overexpression of dominant negative Cullin-3 fragments resulted in decreased synaptic  
698 turnover of AMPA-type glutamate receptor subunits (Schaefer H and Rongo C, 2006). By  
699 contrast, levels of AMPA receptor subunits were unchanged in synaptosome preparations from  
700 heterozygous CUL3 knockout mouse brains, while kainate receptor subunits accumulated by  
701 about 20% (Salinas GD et al., 2006). Little is known about the function of Cullin-3 in human  
702 neurodevelopment. Knockdown of the Cullin-3 adaptor KBTBD8 by short hairpin RNA in

703 human embryonic stem cell cultures did not affect proliferation or pluripotency. Following small  
704 molecule-mediated neural differentiation however, knockdown of KBTBD8 resulted in an  
705 increase in CNS neuronal precursor cells and a decline in neural crest cells (Werner A et al.,  
706 2015).

707 Since fibroblasts from psychiatric patients carrying rare, protein-truncating mutations in the  
708 CUL3 gene were not available for reprogramming, we used CRISPR/Cas9 nickase to knockout  
709 CUL3 in human iPSCs from healthy donors. This approach generates isogenic iPSC lines,  
710 thereby minimizing genetic background heterogeneity (Jinek M et al., 2012; Kim HS et al.,  
711 2014), and reduces off-target effects observed with Cas9 nuclease (Ran FA et al., 2013). By  
712 DNA sequencing, we detected a 3 bp, in-frame deletion in iPSC clone 6, and a 17 bp deletion  
713 in clone 19. Consistent with CUL3 gene targeting in mice (Singer JD et al., 1999), we detected  
714 only heterozygous CUL3 KO iPSC lines. The 17 bp, frameshift deletion in clone 19 is predicted  
715 to lead to a premature stop codon (p.Phe199X), which may result in nonsense-mediated  
716 mRNA decay (Chang YF et al., 2007) of the mutant CUL3 transcript. By contrast, the decrease  
717 in CUL3 mRNA in clone 6 carrying a 3 bp in-frame deletion, is surprising. According to three-  
718 dimensional models of the protein structure of Cullin E3 ligases (Petroski MD and Deshaies  
719 RJ, 2005; Zheng N et al., 2002), the single amino acid (Glu202 or Glu203) deletion of clone 6  
720 is located in an alpha-helix of the Cullin repeat motif. Moreover, amino acids Glu202 and  
721 Glu203 are highly conserved between species. The N-terminal Cullin repeats have a rigid  
722 structure, which is required to juxtapose the protein substrate and the E2 enzyme for ubiquitin  
723 transfer, since mutations that increase flexibility destroyed Cullin E3 activity (Petroski MD and  
724 Deshaies RJ, 2005; Zheng N et al., 2002). It may be hypothesized, that deletion of Glu202 or  
725 Glu203 has a deleterious effect on the structure/rigidity of the Cullin repeat, and consequently  
726 the stability/activity of Cullin-3 (Schumacher FR et al., 2015). Interestingly, similar findings  
727 have been published in the non-related protein Kindlin-1, where an in-frame deletion of a single  
728 amino acid in a highly structured region affected protein structure and led to a massive  
729 reduction of mRNA and protein (Maier K et al., 2016). By immunoblot analyses using two  
730 different anti-Cullin-3 antibodies, we detected an approximate 50% reduction in Cullin-3 protein  
731 levels in the two heterozygous CUL3 KO iPSC clones, and a Cullin-3 band migrating at a  
732 slightly higher molecular weight in CUL3 KO clone 19. It may be speculated that the reduction  
733 in Cullin-3 protein in heterozygous CUL3 KO iPSC leads to an increase in post-translational  
734 modifications (e.g. neddylation, autoubiquitylation) of Cullin-3 encoded by the wildtype allele  
735 (Genschik P et al., 2013; Petroski MD and Deshaies RJ, 2005). Alternatively, structural  
736 changes in the mutant Cullin-3 protein may increase neddylation and autoubiquitylation as  
737 shown by others (Schumacher FR et al., 2015). It remains unclear however, why the shift in  
738 the Cullin-3 protein band is not detectable in the heterozygous CUL3 KO clone 6. An about

739 50% neddylation of Cullin-3 has been detected in mouse embryonic stem cells plated on  
740 gelatin using a different antibody (Jin L et al., 2012). Our immunoblot analyses suggest that  
741 the basal levels of neddylated Cullin-3 are lower in human iPSCs plated on Matrigel. In addition,  
742 differential splicing of CUL3, which has recently been demonstrated both in human NPC  
743 cultures and in the mouse forebrain (Burke EE et al., 2020; Furlanis E et al., 2019), might  
744 contribute to the shift of the Cullin-3 band in our immunoblot analysis.

745 Although CUL3 mRNA is expressed in human iPSCs ((van de Leemput J et al., 2014) and  
746 present study), our heterozygous KO of CUL3 by Cas9 nickase did not affect expression of  
747 various markers for pluripotency, which is consistent with unaltered expression of pluripotency  
748 markers in mouse embryonic stem cells depleted of CUL3 by short interfering RNA treatment  
749 (Jin L et al., 2012). Messenger RNA expression of CUL3 remains at high levels during small  
750 molecule-mediated neuronal differentiation of iPSC ((van de Leemput J et al., 2014) and  
751 present study). At the NPC stage, we detected a moderate increase in cell proliferation of the  
752 three CUL3 KO clones by EdU labeling during DNA replication, which is consistent with  
753 findings in embryonic fibroblasts from heterozygous CUL3 KO mice (McEvoy JD et al., 2007).  
754 To profile expression of genes regulating neuronal development and function, we used 96-well  
755 qPCR arrays. Bulk or single cell RNA-sequencing will be required however, to get a more  
756 complete picture of changes in gene expression and signaling pathways induced by Cullin-3  
757 deficiency. Both by PCR Human Neurogenesis arrays and by qRT-PCR, we detected an  
758 approximate 3-fold increase in PAX6 mRNA levels in heterozygous CUL3 KO NPCs derived  
759 from clone 6 and clone 19. In the embryonic mouse cortex, PAX6 plays an essential role in the  
760 differentiation of radial glia cells (RGCs) (Gotz M et al., 1998), and in cultured mouse  
761 embryonic stem cells, PAX6 knockdown decreased differentiation of neuroepithelial cells to  
762 RGCs (Suter DM et al., 2009). Additionally, we found a moderate decrease in TENM1 mRNA  
763 expression. The protein product, teneurin-1, has a role in synapse organization and neurite  
764 elongation in mice (reviewed in (Mosca TJ, 2015)). By PCR Human Neurotransmitter array  
765 analysis and by qRT-PCR of 14 days old, iPSC-derived neurons, we found a > 3-fold increase  
766 in mRNA levels of the glutamate transporter, solute carrier family 1 member 3 (SLC1A3), in  
767 heterozygous CUL3 KO neurons derived from clone 6 and clone 19. SLC1A3 (EAAT1,  
768 GLAST1) is best known as the astrocytic glutamate transporter, which takes up the  
769 neurotransmitter glutamate after release from neuronal synapses (Hertz L and Zielke HR,  
770 2004). In our iPSC-derived neuron cultures however, astrocytes become detectable only after  
771 45 days of small molecule differentiation ((Shi Y et al., 2012) and present study). By single cell  
772 RNA sequencing of the developing human neocortex, independent studies demonstrated  
773 preferential expression of SLC1A3 in proliferating RGCs and NPCs (Johnson MB et al., 2015;  
774 Polioudakis D et al., 2019; Zhong S et al., 2018). Thus, higher mRNA levels of the RGC/NPC

775 markers PAX6 and SLC1A3 in our heterozygous CUL3 KO cultures may indicate that these  
776 cells are retained in the RGC/NPC stage during small molecule-mediated neuronal  
777 differentiation. Consistently, we observed an appearance of Pax-6 positive NPCs forming  
778 neural rosettes in CUL3 KO neuron cultures. These proliferating CUL3 KO RGCs/NPCs  
779 overgrow the neuron cultures, which resulted in a (seeming) decline in neuronal electrical  
780 activity during our MEA recordings. Higher levels of PAX6 mRNA expression and higher  
781 numbers of Pax6-positive RGCs/NPCs in heterozygous CUL3 KO clone 8 compared to KO  
782 clone 19 might be partially explained by lower levels of CUL3 protein expression and protein  
783 modification in clone 8. However, since genomic instability has been reported in several iPSC  
784 studies (reviewed in (Drakulic D et al., 2020)), we cannot formally exclude a contribution by  
785 small genomic alterations that escaped detection by our array-based karyotype analysis and  
786 that can only be ruled out by whole genome sequencing. It should be noted, that we did not  
787 add antimitotic agents, like cytosine arabinoside (Ara-C), to our cultures of iPSC-derived  
788 neurons. Ara-C has been added to the medium in other iPSC studies to inhibit proliferation of  
789 non-neuronal cells and cocultured astrocytes, but Ara-C may also prevent growth of persisting  
790 RGCs/NPCs during neuronal differentiation in iPSC models of neurodevelopmental disorders.  
791 Increased expression of marker genes for immature neurons, a decrease in spontaneous  
792 neuronal network activity over time, and impaired synaptic plasticity were also detected in  
793 iPSC-derived cortical neurons of patients diagnosed with ASD, Angelman syndrome, and  
794 childhood-onset schizophrenia, respectively (Fink JJ et al., 2017; Flaherty E et al., 2019;  
795 Marchetto MC et al., 2017). Taken together, there is increasing evidence that deficits in  
796 neuronal differentiation are a point of convergence in iPSC models of  
797 neurodevelopmental/neuropsychiatric disorders (reviewed in (Ahmad R et al., 2018; Ernst C,  
798 2016; Ichida JK and Kiskinis E, 2015)). These neurodevelopmental deficits may be  
799 exacerbated (e.g. overgrowth of iPSC-derived neurons by persisting RGCs/NPCs in the  
800 present study) in iPSC models grown in two-dimensional culture on exogenous extracellular  
801 matrix, however, numerous neuropathological studies of postmortem cortical tissue from  
802 autistic children revealed signs of extended neurogenesis, neuronal immaturity, and abnormal  
803 migration consistent with dysregulation of neuronal differentiation at prenatal stages (Kaushik  
804 G and Zarbalis KS, 2016; Stoner R et al., 2014; Wegiel J et al., 2010).

805 Lentiviral expression of the neuralizing transcription factor NGN2 directly converts human  
806 iPSCs into cortical glutamatergic neurons and appears to circumvent the NPC stage (Zhang Y  
807 et al., 2013). By RNA sequencing robust CUL3 expression has been demonstrated at all time-  
808 points of direct neuronal conversion, while SLC1A3 expression could not be detected ((Tian R  
809 et al., 2019) and present study). Overexpression of NGN2 in RGCs of the developing ferret  
810 cortex shifts RGCs into postmitotic neurons (Johnson MB et al., 2015). These data might

811 explain, why the persistence of RGCs/NPCs in CUL3 KO cultures during small molecule-  
812 mediated neuronal differentiation was not observed during NGN2-mediated direct neuronal  
813 conversion in our study. Our findings also sound a note of caution. Risk genes for  
814 neurodevelopmental/neuropsychiatric disorders are significantly enriched in RGCs/NPCs of  
815 the prenatal human neocortex (Polioudakis D et al., 2019; Schork AJ et al., 2019), and non-  
816 coding risk variants have been identified in human-specific enhancers that regulate the  
817 proliferation of outer RGCs. This cell type is particularly important for the evolutionary  
818 expansion of the human neocortex and the increased cognitive abilities of humans (de la Torre-  
819 Ubieta L et al., 2018). Therefore, disease-relevant, early neurodevelopmental alterations  
820 induced by these risk genes in iPSC models may be obscured by direct neuronal conversion,  
821 which bypasses the RGC/NPC stage. Similar findings have recently been reported in iPSCs  
822 from idiopathic, macrocephalic ASD patients, where NGN2-mediated direct conversion  
823 attenuated ASD-associated accelerated neurite outgrowth observed during small molecule  
824 differentiation (Schafer ST et al., 2019).

825 However, non-coding common variants for SZ form contacts with the CUL3 gene in NGN2-  
826 induced neurons (Rajarajan P et al., 2018) indicating that (patho-)physiological neuronal  
827 functions of Cullin-3 can be identified in induced cortical glutamatergic neurons. Although our  
828 multiparametric analysis of MEA recordings did not reveal significant differences in  
829 spontaneous spikes, bursts, and networks bursts between induced CUL3 KO neurons and  
830 isogenic controls, both optogenetic stimulation combined with MEA recordings and electrical  
831 stimulation combined with calcium imaging demonstrated a significant decrease in neuronal  
832 excitability. The rapid decline in evoked activity in CUL3 KO neurons after 5 light pulses may  
833 indicate enhanced short-term synaptic depression and/or accelerated depletion of readily  
834 releasable synaptic vesicles in glutamatergic synapses. Consistently, normal basal synaptic  
835 transmission and altered short-term synaptic plasticity have been reported in cortical pyramidal  
836 neurons of various genetic mouse models of SZ/ASD (reviewed in (Crabtree GW and Gogos  
837 JA, 2014)). Very recently, decreased excitability and spine loss has also been detected in  
838 cortical pyramidal neurons of heterozygous mice with forebrain-specific CUL3 deletion  
839 (Rapanelli M et al., 2019). Thus, both human iPSC models and mutant mouse models exhibit  
840 deficits in cortical glutamatergic signaling, which may represent one of the earliest  
841 pathophysiological alteration in schizophrenia (Krystal JH et al., 2017).

842 Signaling via both the Notch receptor and the FGF receptor is crucial for maintenance of NPCs  
843 in an undifferentiated, self-renewing state (reviewed in (Guillemot F and Zimmer C, 2011;  
844 Mason I, 2007; Pierfelice T et al., 2011)). Since both signaling cascades are regulated by Cullin  
845 E3 ligases (Guillemot F and Zimmer C, 2011; Mason I, 2007; Matsumoto A et al., 2011), we  
846 investigated the expression of known target genes of Notch and FGF, respectively, in

847 proliferating NPC cultures. While Notch target gene expression was unaltered in heterozygous  
848 CUL3 KO NPCs, expression of feedback inhibitors of FGF signaling (SPRY1, IL17RD) was  
849 significantly reduced. Interestingly, human brain-specific gene network analysis identified  
850 FGF1 and FGFR2 as key intermediate genes linking high confidence ASD genes to disorder-  
851 related pathways (Krishnan A et al., 2016). Moreover, by gene expression profiling increased  
852 FGF2 mRNA expression was detected in the temporal cortex of autism patients (Garbett K et  
853 al., 2008). Although further studies are required to clarify whether Cullin-3 deficiency directly  
854 or indirectly affects FGF signaling, our study indicates that Cullin-3 ubiquitin ligase regulates  
855 differentiation of human cortical RGCs/NPCs, which might contribute to the  
856 neurodevelopmental deficits in psychiatric disorders associated with CUL3 loss-of-function  
857 mutations.

858

859

### 860 **Acknowledgements**

861 The authors thank Selina Reich for nucleofection of iPSCs, Dr. Stefan Jäger for help with digital  
862 image analysis, Dr. Bernd-Wolfgang Igl (all Boehringer Ingelheim Pharma GmbH & Co. KG,  
863 Biberach, Germany) for expert advice concerning statistical analysis, and Prof. Vania Broccoli  
864 (Ospedale San Raffaele, Milan, Italy) for providing lentiviral vectors.

865

866

### 867 **Abbreviations**

868 ASD, autism spectrum disorder; Cas9n, Cas9 nickase; GWAS, genome-wide association  
869 study; iPSC, induced pluripotent stem cell; NPC, neural precursor cell; qRT-PCR, quantitative  
870 real time PCR; RGC, radial glia cell; SZ, schizophrenia

871 **REFERENCES**

- 872
- 873 Ahmad R, Sportelli V, Ziller M, Spengler D, Hoffmann A (2018), Tracing Early  
874 Neurodevelopment in Schizophrenia with Induced Pluripotent Stem Cells. *Cells* 7.
- 875 Bahari-Javan S, Varbanov H, Halder R, Benito E, Kaurani L, Burkhardt S, Anderson-Schmidt H,  
876 Anghelescu I, et al. (2017), HDAC1 links early life stress to schizophrenia-like phenotypes. *Proc*  
877 *Natl Acad Sci U S A* 114:E4686-e4694.
- 878 Brennand K, Savas JN, Kim Y, Tran N, Simone A, Hashimoto-Torii K, Beaumont KG, Kim HJ, et  
879 al. (2015), Phenotypic differences in hiPSC NPCs derived from patients with schizophrenia. *Mol*  
880 *Psychiatry* 20:361-368.
- 881 Brennand KJ, Simone A, Jou J, Gelboin-Burkhart C, Tran N, Sangar S, Li Y, Mu Y, et al. (2011),  
882 Modelling schizophrenia using human induced pluripotent stem cells. *Nature* 473:221-225.
- 883 Burke EE, Chenoweth JG, Shin JH, Collado-Torres L, Kim SK, Micali N, Wang Y, Colantuoni C, et  
884 al. (2020), Dissecting transcriptomic signatures of neuronal differentiation and maturation  
885 using iPSCs. *Nat Commun* 11:462.
- 886 Chambers SM, Fasano CA, Papapetrou EP, Tomishima M, Sadelain M, Studer L (2009), Highly  
887 efficient neural conversion of human ES and iPS cells by dual inhibition of SMAD signaling. *Nat*  
888 *Biotechnol* 27:275-280.
- 889 Chang YF, Imam JS, Wilkinson MF (2007), The nonsense-mediated decay RNA surveillance  
890 pathway. *Annu Rev Biochem* 76:51-74.
- 891 Chen Y, Yang Z, Meng M, Zhao Y, Dong N, Yan H, Liu L, Ding M, et al. (2009), Cullin mediates  
892 degradation of RhoA through evolutionarily conserved BTB adaptors to control actin  
893 cytoskeleton structure and cell movement. *Mol Cell* 35:841-855.
- 894 Clements IP, Millard DC, Nicolini AM, Preyer AJ, Grier R, Heckerling A, Blum RA, Tyler P, et al.  
895 (2016) Optogenetic stimulation of multiwell MEA plates for neural and cardiac applications.  
896 *SPIE*.
- 897 Codina-Sola M, Rodriguez-Santiago B, Homs A, Santoyo J, Rigau M, Aznar-Lain G, Del Campo  
898 M, Gener B, et al. (2015), Integrated analysis of whole-exome sequencing and transcriptome  
899 profiling in males with autism spectrum disorders. *Mol Autism* 6:21.
- 900 Colasante G, Lignani G, Rubio A, Medrihan L, Yekhlief L, Sessa A, Massimino L, Giannelli SG, et  
901 al. (2015), Rapid Conversion of Fibroblasts into Functional Forebrain GABAergic Interneurons  
902 by Direct Genetic Reprogramming. *Cell Stem Cell* 17:719-734.
- 903 Crabtree GW, Gogos JA (2014), Synaptic plasticity, neural circuits, and the emerging role of  
904 altered short-term information processing in schizophrenia. *Frontiers in synaptic*  
905 *neuroscience* 6:28.
- 906 da Silva Montenegro EM, Costa CS, Campos G, Scliar M, de Almeida TF, Zachi EC, Silva IMW,  
907 Chan AJS, et al. (2019), Meta-Analyses Support Previous and Novel Autism Candidate Genes:  
908 Outcomes of an Unexplored Brazilian Cohort. *Autism research : official journal of the*  
909 *International Society for Autism Research*.
- 910 de la Torre-Ubieta L, Stein JL, Won H, Opland CK, Liang D, Lu D, Geschwind DH (2018), The  
911 Dynamic Landscape of Open Chromatin during Human Cortical Neurogenesis. *Cell* 172:289-  
912 304.e218.
- 913 Drakulic D, Djurovic S, Syed YA, Trattaro S, Caporale N, Falk A, Ofir R, Heine VM, et al. (2020),  
914 Copy number variants (CNVs): a powerful tool for iPSC-based modelling of ASD. *Mol Autism*  
915 11:42.

- 916 Ernst C (2016), Proliferation and Differentiation Deficits are a Major Convergence Point for  
917 Neurodevelopmental Disorders. *Trends in neurosciences* 39:290-299.
- 918 Fink JJ, Robinson TM, Germain ND, Sirois CL, Bolduc KA, Ward AJ, Rigo F, Chamberlain SJ, et al.  
919 (2017), Disrupted neuronal maturation in Angelman syndrome-derived induced pluripotent  
920 stem cells. *Nat Commun* 8:15038.
- 921 Flaherty E, Zhu S, Barretto N, Cheng E, Deans PJM, Fernando MB, Schrode N, Francoeur N, et  
922 al. (2019), Neuronal impact of patient-specific aberrant NRXN1alpha splicing. *Nat Genet*  
923 51:1679-1690.
- 924 Forrest MP, Zhang H, Moy W, McGowan H, Leites C, Dionisio LE, Xu Z, Shi J, et al. (2017), Open  
925 Chromatin Profiling in hiPSC-Derived Neurons Prioritizes Functional Noncoding Psychiatric  
926 Risk Variants and Highlights Neurodevelopmental Loci. *Cell Stem Cell* 21:305-318 e308.
- 927 Forrest MP, Zhang H, Moy W, McGowan H, Leites C, Dionisio LE, Xu Z, Shi J, et al. (2017), Open  
928 Chromatin Profiling in hiPSC-Derived Neurons Prioritizes Functional Noncoding Psychiatric  
929 Risk Variants and Highlights Neurodevelopmental Loci. *Cell Stem Cell* 21:305-318.e308.
- 930 Furlanis E, Traunmuller L, Fucile G, Scheiffele P (2019), Landscape of ribosome-engaged  
931 transcript isoforms reveals extensive neuronal-cell-class-specific alternative splicing programs.  
932 *Nature neuroscience* 22:1709-1717.
- 933 Garbett K, Ebert PJ, Mitchell A, Lintas C, Manzi B, Mirnics K, Persico AM (2008), Immune  
934 transcriptome alterations in the temporal cortex of subjects with autism. *Neurobiology of*  
935 *disease* 30:303-311.
- 936 Genschik P, Sumara I, Lechner E (2013), The emerging family of CULLIN3-RING ubiquitin ligases  
937 (CRL3s): cellular functions and disease implications. *Embo j* 32:2307-2320.
- 938 Gotz M, Stoykova A, Gruss P (1998), Pax6 controls radial glia differentiation in the cerebral  
939 cortex. *Neuron* 21:1031-1044.
- 940 Guillemot F, Zimmer C (2011), From cradle to grave: the multiple roles of fibroblast growth  
941 factors in neural development. *Neuron* 71:574-588.
- 942 Hershko A, Ciechanover A (1998), The ubiquitin system. *Annu Rev Biochem* 67:425-479.
- 943 Hertz L, Zielke HR (2004), Astrocytic control of glutamatergic activity: astrocytes as stars of the  
944 show. *Trends in neurosciences* 27:735-743.
- 945 Ichida JK, Kiskinis E (2015), Probing disorders of the nervous system using reprogramming  
946 approaches. *Embo j* 34:1456-1477.
- 947 Jerabkova K, Sumara I (2018), Cullin 3, a cellular scripter of the non-proteolytic ubiquitin code.  
948 *Seminars in cell & developmental biology*.
- 949 Jin L, Pahuja KB, Wickliffe KE, Gorur A, Baumgartel C, Schekman R, Rape M (2012), Ubiquitin-  
950 dependent regulation of COPII coat size and function. *Nature* 482:495-500.
- 951 Jinek M, Chylinski K, Fonfara I, Hauer M, Doudna JA, Charpentier E (2012), A programmable  
952 dual-RNA-guided DNA endonuclease in adaptive bacterial immunity. *Science* 337:816-821.
- 953 Johnson MB, Wang PP, Atabay KD, Murphy EA, Doan RN, Hecht JL, Walsh CA (2015), Single-  
954 cell analysis reveals transcriptional heterogeneity of neural progenitors in human cortex.  
955 *Nature neuroscience* 18:637-646.
- 956 Kang HJ, Kawasawa YI, Cheng F, Zhu Y, Xu X, Li M, Sousa AM, Pletikos M, et al. (2011), Spatio-  
957 temporal transcriptome of the human brain. *Nature* 478:483-489.
- 958 Kaushik G, Zarbalis KS (2016), Prenatal Neurogenesis in Autism Spectrum Disorders. *Frontiers*  
959 *in chemistry* 4:12.



- 960 Kikuma K, Li X, Perry S, Li Q, Goel P, Chen C, Kim D, Stavropoulos N, et al. (2019), Cul3 and  
961 insomniac are required for rapid ubiquitination of postsynaptic targets and retrograde  
962 homeostatic signaling. *Nat Commun* 10:2998.
- 963 Kim HS, Bernitz JM, Lee DF, Lemischka IR (2014), Genomic editing tools to model human  
964 diseases with isogenic pluripotent stem cells. *Stem Cells Dev* 23:2673-2686.
- 965 Kizner V, Naujock M, Fischer S, Jager S, Reich S, Schlotthauer I, Zuckschwerdt K, Geiger T, et  
966 al. (2019), CRISPR/Cas9-mediated Knockout of the Neuropsychiatric Risk Gene KCTD13 Causes  
967 Developmental Deficits in Human Cortical Neurons Derived from Induced Pluripotent Stem  
968 Cells. *Mol Neurobiol*.
- 969 Kizner V, Naujock M, Fischer S, Jäger S, Reich S, Schlotthauer I, Zuckschwerdt K, Geiger T, et  
970 al. (2019), CRISPR/Cas9-mediated Knockout of the Neuropsychiatric Risk Gene KCTD13 Causes  
971 Developmental Deficits in Human Cortical Neurons Derived from Induced Pluripotent Stem  
972 Cells. *Mol Neurobiol*.
- 973 Kong A, Frigge ML, Masson G, Besenbacher S, Sulem P, Magnusson G, Gudjonsson SA,  
974 Sigurdsson A, et al. (2012), Rate of de novo mutations and the importance of father's age to  
975 disease risk. *Nature* 488:471-475.
- 976 Krishnan A, Zhang R, Yao V, Theesfeld CL, Wong AK, Tadych A, Volfovsky N, Packer A, et al.  
977 (2016), Genome-wide prediction and functional characterization of the genetic basis of autism  
978 spectrum disorder. *Nature neuroscience* 19:1454-1462.
- 979 Krystal JH, Anticevic A, Yang GJ, Dragoi G, Driesen NR, Wang XJ, Murray JD (2017), Impaired  
980 Tuning of Neural Ensembles and the Pathophysiology of Schizophrenia: A Translational and  
981 Computational Neuroscience Perspective. *Biol Psychiatry* 81:874-885.
- 982 Kyttala A, Moraghebi R, Valensisi C, Kettunen J, Andrus C, Pasumarthy KK, Nakanishi M,  
983 Nishimura K, et al. (2016), Genetic Variability Overrides the Impact of Parental Cell Type and  
984 Determines iPSC Differentiation Potential. *Stem Cell Reports* 6:200-212.
- 985 Lek M, Karczewski KJ, Minikel EV, Samocha KE, Banks E, Fennell T, O'Donnell-Luria AH, Ware  
986 JS, et al. (2016), Analysis of protein-coding genetic variation in 60,706 humans. *Nature*  
987 536:285-291.
- 988 Lewis DA, Gonzalez-Burgos G (2006), Pathophysiologically based treatment interventions in  
989 schizophrenia. *Nat Med* 12:1016-1022.
- 990 Li M, Santpere G, Imamura Kawasawa Y, Evgrafov OV, Gulden FO, Pochareddy S, Sunkin SM,  
991 Li Z, et al. (2018), Integrative functional genomic analysis of human brain development and  
992 neuropsychiatric risks. *Science* 362.
- 993 Lin GN, Corominas R, Lemmens I, Yang X, Tavernier J, Hill DE, Vidal M, Sebat J, et al. (2015),  
994 Spatiotemporal 16p11.2 protein network implicates cortical late mid-fetal brain development  
995 and KCTD13-Cul3-RhoA pathway in psychiatric diseases. *Neuron* 85:742-754.
- 996 Maier K, He Y, Esser PR, Thriene K, Sarca D, Kohlhase J, Dengjel J, Martin L, et al. (2016), Single  
997 Amino Acid Deletion in Kindlin-1 Results in Partial Protein Degradation Which Can Be Rescued  
998 by Chaperone Treatment. *The Journal of investigative dermatology* 136:920-929.
- 999 Marchetto MC, Belinson H, Tian Y, Freitas BC, Fu C, Vadodaria K, Beltrao-Braga P, Trujillo CA,  
1000 et al. (2017), Altered proliferation and networks in neural cells derived from idiopathic autistic  
1001 individuals. *Mol Psychiatry* 22:820-835.
- 1002 Marchetto MC, Carromeu C, Acab A, Yu D, Yeo GW, Mu Y, Chen G, Gage FH, et al. (2010), A  
1003 model for neural development and treatment of Rett syndrome using human induced  
1004 pluripotent stem cells. *Cell* 143:527-539.

- 1005 Mason I (2007), Initiation to end point: the multiple roles of fibroblast growth factors in neural  
1006 development. *Nat Rev Neurosci* 8:583-596.
- 1007 Matsumoto A, Onoyama I, Sunabori T, Kageyama R, Okano H, Nakayama KI (2011), Fbxw7-  
1008 dependent degradation of Notch is required for control of "stemness" and neuronal-glia  
1009 differentiation in neural stem cells. *J Biol Chem* 286:13754-13764.
- 1010 McEvoy JD, Kossatz U, Malek N, Singer JD (2007), Constitutive turnover of cyclin E by Cul3  
1011 maintains quiescence. *Mol Cell Biol* 27:3651-3666.
- 1012 Millan MJ, Andrieux A, Bartzokis G, Cadenhead K, Dazzan P, Fusar-Poli P, Gallinat J, Giedd J, et  
1013 al. (2016), Altering the course of schizophrenia: progress and perspectives. *Nat Rev Drug*  
1014 *Discov* 15:485-515.
- 1015 Morrison M, Klein C, Clemann N, Collier DA, Hardy J, Heisserer B, Cader MZ, Graf M, et al.  
1016 (2015), StemBANCC: Governing Access to Material and Data in a Large Stem Cell Research  
1017 Consortium. *Stem Cell Rev* 11:681-687.
- 1018 Mosca TJ (2015), On the Teneurin track: a new synaptic organization molecule emerges. *Front*  
1019 *Cell Neurosci* 9:204.
- 1020 Murai K, Sun G, Ye P, Tian E, Yang S, Cui Q, Sun G, Trinh D, et al. (2016), The TLX-miR-219  
1021 cascade regulates neural stem cell proliferation in neurodevelopment and schizophrenia iPSC  
1022 model. *Nat Commun* 7:10965.
- 1023 Nehme R, Zuccaro E, Ghosh SD, Li C, Sherwood JL, Pietilainen O, Barrett LE, Limone F, et al.  
1024 (2018), Combining NGN2 Programming with Developmental Patterning Generates Human  
1025 Excitatory Neurons with NMDAR-Mediated Synaptic Transmission. *Cell Rep* 23:2509-2523.
- 1026 O'Roak BJ, Vives L, Girirajan S, Karakoc E, Krumm N, Coe BP, Levy R, Ko A, et al. (2012), Sporadic  
1027 autism exomes reveal a highly interconnected protein network of de novo mutations. *Nature*  
1028 485:246-250.
- 1029 Pak C, Danko T, Zhang Y, Aoto J, Anderson G, Maxeiner S, Yi F, Wernig M, et al. (2015), Human  
1030 Neuropsychiatric Disease Modeling using Conditional Deletion Reveals Synaptic Transmission  
1031 Defects Caused by Heterozygous Mutations in NRXN1. *Cell Stem Cell* 17:316-328.
- 1032 Pardinias AF, Holmans P, Pocklington AJ, Escott-Price V, Ripke S, Carrera N, Legge SE, Bishop S,  
1033 et al. (2018), Common schizophrenia alleles are enriched in mutation-intolerant genes and in  
1034 regions under strong background selection. *Nat Genet* 50:381-389.
- 1035 Pasca SP, Portmann T, Voineagu I, Yazawa M, Shcheglovitov A, Pasca AM, Cord B, Palmer TD,  
1036 et al. (2011), Using iPSC-derived neurons to uncover cellular phenotypes associated with  
1037 Timothy syndrome. *Nat Med* 17:1657-1662.
- 1038 Petroski MD, Deshaies RJ (2005), Function and regulation of cullin-RING ubiquitin ligases. *Nat*  
1039 *Rev Mol Cell Biol* 6:9-20.
- 1040 Pierfelice T, Alberi L, Gaiano N (2011), Notch in the vertebrate nervous system: an old dog  
1041 with new tricks. *Neuron* 69:840-855.
- 1042 Polioudakis D, de la Torre-Ubieta L, Langerman J, Elkins AG, Shi X, Stein JL, Vuong CK,  
1043 Nichterwitz S, et al. (2019), A Single-Cell Transcriptomic Atlas of Human Neocortical  
1044 Development during Mid-gestation. *Neuron* 103:785-801.e788.
- 1045 Qi Y, Zhang XJ, Renier N, Wu Z, Atkin T, Sun Z, Ozair MZ, Tchieu J, et al. (2017), Combined small-  
1046 molecule inhibition accelerates the derivation of functional cortical neurons from human  
1047 pluripotent stem cells. *Nat Biotechnol* 35:154-163.
- 1048 Rajarajan P, Borrmann T, Liao W, Schrode N, Flaherty E, Casiño C, Powell S, Yashaswini C, et al.  
1049 (2018), Neuron-specific signatures in the chromosomal connectome associated with  
1050 schizophrenia risk. *Science* 362:eaat4311.

- 1051 Ran FA, Hsu PD, Lin CY, Gootenberg JS, Konermann S, Trevino AE, Scott DA, Inoue A, et al.  
1052 (2013), Double nicking by RNA-guided CRISPR Cas9 for enhanced genome editing specificity.  
1053 *Cell* 154:1380-1389.
- 1054 Rapanelli M, Tan T, Wang W, Wang X, Wang ZJ, Zhong P, Frick L, Qin L, et al. (2019), Behavioral,  
1055 circuitry, and molecular aberrations by region-specific deficiency of the high-risk autism gene  
1056 *Cul3*. *Mol Psychiatry*.
- 1057 Ruzzo EK, Perez-Cano L, Jung JY, Wang LK, Kashef-Haghighi D, Hartl C, Singh C, Xu J, et al. (2019),  
1058 Inherited and De Novo Genetic Risk for Autism Impacts Shared Networks. *Cell* 178:850-  
1059 866.e826.
- 1060 Salinas GD, Blair LA, Needleman LA, Gonzales JD, Chen Y, Li M, Singer JD, Marshall J (2006),  
1061 Actinfilin is a *Cul3* substrate adaptor, linking *GluR6* kainate receptor subunits to the ubiquitin-  
1062 proteasome pathway. *J Biol Chem* 281:40164-40173.
- 1063 Schaefer H, Rongo C (2006), *KEL-8* is a substrate receptor for *CUL3*-dependent ubiquitin ligase  
1064 that regulates synaptic glutamate receptor turnover. *Molecular biology of the cell* 17:1250-  
1065 1260.
- 1066 Schafer ST, Paquola ACM, Stern S, Gosselin D, Ku M, Pena M, Kuret TJM, Liyanage M, et al.  
1067 (2019), Pathological priming causes developmental gene network heterochronicity in autistic  
1068 subject-derived neurons. *Nature neuroscience* 22:243-255.
- 1069 Schizophrenia Working Group of the Psychiatric Genomics C (2014), Biological insights from  
1070 108 schizophrenia-associated genetic loci. *Nature* 511:421-427.
- 1071 Schork AJ, Won H, Appadurai V, Nudel R, Gandal M, Delaneau O, Revsbech Christiansen M,  
1072 Hougaard DM, et al. (2019), A genome-wide association study of shared risk across psychiatric  
1073 disorders implicates gene regulation during fetal neurodevelopment. *Nature neuroscience*  
1074 22:353-361.
- 1075 Schumacher FR, Siew K, Zhang J, Johnson C, Wood N, Cleary SE, Al Maskari RS, Ferryman JT, et  
1076 al. (2015), Characterisation of the *Cullin-3* mutation that causes a severe form of familial  
1077 hypertension and hyperkalaemia. *EMBO Mol Med* 7:1285-1306.
- 1078 Sheridan SD, Theriault KM, Reis SA, Zhou F, Madison JM, Daheron L, Loring JF, Haggarty SJ  
1079 (2011), Epigenetic characterization of the *FMR1* gene and aberrant neurodevelopment in  
1080 human induced pluripotent stem cell models of fragile X syndrome. *PLoS One* 6:e26203.
- 1081 Shi Y, Kirwan P, Livesey FJ (2012), Directed differentiation of human pluripotent stem cells to  
1082 cerebral cortex neurons and neural networks. *Nature protocols* 7:1836-1846.
- 1083 Shi Y, Kirwan P, Smith J, Robinson HP, Livesey FJ (2012), Human cerebral cortex development  
1084 from pluripotent stem cells to functional excitatory synapses. *Nat Neurosci* 15:477-486, S471.
- 1085 Singer JD, Gurian-West M, Clurman B, Roberts JM (1999), *Cullin-3* targets cyclin E for  
1086 ubiquitination and controls S phase in mammalian cells. *Genes & development* 13:2375-2387.
- 1087 Song M, Yang X, Ren X, Maliskova L, Li B, Jones IR, Wang C, Jacob F, et al. (2019), Mapping cis-  
1088 regulatory chromatin contacts in neural cells links neuropsychiatric disorder risk variants to  
1089 target genes. *Nat Genet* 51:1252-1262.
- 1090 Stoner R, Chow ML, Boyle MP, Sunkin SM, Mouton PR, Roy S, Wynshaw-Boris A, Colamarino  
1091 SA, et al. (2014), Patches of disorganization in the neocortex of children with autism. *N Engl J*  
1092 *Med* 370:1209-1219.
- 1093 Sullivan PF, Kendler KS, Neale MC (2003), Schizophrenia as a complex trait: evidence from a  
1094 meta-analysis of twin studies. *Arch Gen Psychiatry* 60:1187-1192.

- 1095 Suter DM, Tirefort D, Julien S, Krause KH (2009), A Sox1 to Pax6 switch drives neuroectoderm  
1096 to radial glia progression during differentiation of mouse embryonic stem cells. *Stem cells*  
1097 (Dayton, Ohio) 27:49-58.
- 1098 Tian R, Gachechiladze MA, Ludwig CH, Laurie MT, Hong JY, Nathaniel D, Prabhu AV,  
1099 Fernandopulle MS, et al. (2019), CRISPR Interference-Based Platform for Multimodal Genetic  
1100 Screens in Human iPSC-Derived Neurons. *Neuron*.
- 1101 Tian R, Gachechiladze MA, Ludwig CH, Laurie MT, Hong JY, Nathaniel D, Prabhu AV,  
1102 Fernandopulle MS, et al. (2019), CRISPR-based platform for multimodal genetic screens in  
1103 human iPSC-derived neurons. *bioRxiv:513309*.
- 1104 van de Leemput J, Boles NC, Kiehl TR, Corneo B, Lederman P, Menon V, Lee C, Martinez RA, et  
1105 al. (2014), CORTECON: a temporal transcriptome analysis of in vitro human cerebral cortex  
1106 development from human embryonic stem cells. *Neuron* 83:51-68.
- 1107 Walsh T, McClellan JM, McCarthy SE, Addington AM, Pierce SB, Cooper GM, Nord AS, Kusenda  
1108 M, et al. (2008), Rare structural variants disrupt multiple genes in neurodevelopmental  
1109 pathways in schizophrenia. *Science* 320:539-543.
- 1110 Wang C, Ward ME, Chen R, Liu K, Tracy TE, Chen X, Xie M, Sohn PD, et al. (2017), Scalable  
1111 Production of iPSC-Derived Human Neurons to Identify Tau-Lowering Compounds by High-  
1112 Content Screening. *Stem Cell Reports* 9:1221-1233.
- 1113 Waterhouse A, Bertoni M, Bienert S, Studer G, Tauriello G, Gumienny R, Heer FT, de Beer TAP,  
1114 et al. (2018), SWISS-MODEL: homology modelling of protein structures and complexes. *Nucleic  
1115 acids research* 46:W296-w303.
- 1116 Wegiel J, Kuchna I, Nowicki K, Imaki H, Wegiel J, Marchi E, Ma SY, Chauhan A, et al. (2010), The  
1117 neuropathology of autism: defects of neurogenesis and neuronal migration, and dysplastic  
1118 changes. *Acta neuropathologica* 119:755-770.
- 1119 Werner A, Iwasaki S, McGourty CA, Medina-Ruiz S, Teerikorpi N, Fedrigo I, Ingolia NT, Rape M  
1120 (2015), Cell-fate determination by ubiquitin-dependent regulation of translation. *Nature*  
1121 525:523-527.
- 1122 Willsey AJ, Sanders SJ, Li M, Dong S, Tebbenkamp AT, Muhle RA, Reilly SK, Lin L, et al. (2013),  
1123 Coexpression networks implicate human midfetal deep cortical projection neurons in the  
1124 pathogenesis of autism. *Cell* 155:997-1007.
- 1125 Zhang Y, Pak C, Han Y, Ahlenius H, Zhang Z, Chanda S, Marro S, Patzke C, et al. (2013), Rapid  
1126 single-step induction of functional neurons from human pluripotent stem cells. *Neuron*  
1127 78:785-798.
- 1128 Zheng N, Schulman BA, Song L, Miller JJ, Jeffrey PD, Wang P, Chu C, Koepf DM, et al. (2002),  
1129 Structure of the Cul1-Rbx1-Skp1-F boxSkp2 SCF ubiquitin ligase complex. *Nature* 416:703-709.
- 1130 Zhong S, Zhang S, Fan X, Wu Q, Yan L, Dong J, Zhang H, Li L, et al. (2018), A single-cell RNA-seq  
1131 survey of the developmental landscape of the human prefrontal cortex. *Nature* 555:524-528.
- 1132 Zhu S, Perez R, Pan M, Lee T (2005), Requirement of Cul3 for axonal arborization and dendritic  
1133 elaboration in *Drosophila* mushroom body neurons. *J Neurosci* 25:4189-4197.
- 1134

1135 **Figure Legends**

1136

1137 **Fig. 1.** CRISPR/Cas9 nickase mediated CUL3 knockout in human induced pluripotent stem  
1138 cells. (A) Identification of CRISPR/Cas9 nickase induced insertions/deletions in the CUL3 gene  
1139 by T7 endonuclease cleavage assay. M, DNA marker; +/+\_4, wildtype, parental control iPSC  
1140 line CB4; +/+\_2 and +/+\_13, Cas9/gRNA-transfected, non-edited, wildtype iPSC clones 2 and  
1141 13, respectively; +/-\_6 and +/-\_19, Cas9/gRNA-transfected, heterozygous CUL3 knockout (KO)  
1142 clones 6 and 19, respectively. (B) Quantitative RT-PCR analysis shows significantly decreased  
1143 CUL3 mRNA expression in heterozygous CUL3 KO iPSC clones 6 and 19 (black boxes)  
1144 compared to isogenic wildtype iPSC clones. Data from two independent experiments and three  
1145 iPSC cultures per clone are shown in box-and whiskers plots. The box depicts the median and  
1146 the 25th and 75th quartiles, and the whiskers show the 5th and 95th percentile. \*\* $p \leq 0.01$ , \*\*\* $p$   
1147  $\leq 0.001$ , unpaired Welch's t-tests. Additional information on statistical analysis is given in  
1148 Supplementary Table S2. (C) DNA sequencing reveals an in-frame, 3 base pair deletion in  
1149 heterozygous CUL3 KO iPSC clone 6 (+/-\_6), and a 17 base pair deletion in heterozygous  
1150 CUL3 KO iPSC clone 19 (+/-\_19).

1151

1152 **Fig. 2.** Immunoblot analysis of Cullin-3 protein levels in iPSC lysates. (A) Representative  
1153 immunoblots showing a decrease in Cullin-3 protein (black arrow) in heterozygous CUL3 KO  
1154 iPSC, and a shift in the Cullin-3 band towards a higher molecular weight in heterozygous CUL3  
1155 KO clone 19. M, protein markers (colorimetric detection); +/+\_4, wildtype, parental control  
1156 iPSC line CB4; +/+\_2 and +/+\_13, Cas9/gRNA-transfected, non-edited, wildtype iPSC clones  
1157 2 and 13, respectively; +/-\_6 and +/-\_19, Cas9/gRNA-transfected, heterozygous CUL3  
1158 knockout (KO) clones 6 and 19, respectively. Both a monoclonal anti-Cullin-3 antibody raised  
1159 against the N-terminus of human Cullin-3 (upper panel) and a polyclonal anti-Cullin-3 antibody  
1160 raised against the C-terminus of human Cullin-3 were used for chemiluminescence detection.  
1161 Immunoblot analysis of beta-Actin (lower panel) and reversible total protein staining of the  
1162 membrane (panel on the right) confirm similar protein loading. (B) Densitometric analysis of all  
1163 immunoblots shows a significant decrease in Cullin-3 protein levels in heterozygous CUL3 KO  
1164 iPSC lines (black boxes) compared to isogenic WT control lines. Data from four independent  
1165 experiments are shown in box-and whiskers plots. The box depicts the median and the 25th  
1166 and 75th quartiles, and the whiskers show the 5th and 95th percentile. \* $p \leq 0.05$ , \*\* $p \leq 0.01$ ,  
1167 unpaired Welch's t-tests. Additional information on statistical analysis is given in  
1168 Supplementary Table S2.

1169

1170 **Fig. 3.** CUL3 deficiency does not affect stemness of iPSC lines. Representative microscopic  
1171 images of immunostainings for stemness markers Oct-4 and Tra-1-60 in iPSC cultures. Nuclei  
1172 were stained with Hoechst 33342 and confocal images were analyzed using an Opera Phenix  
1173 high-content image analysis system. Scale bars represent 100  $\mu\text{m}$ . Data are given in the  
1174 Results section.

1175

1176 **Fig. 4.** Effect of CUL3 deficiency on cell proliferation. (A) Representative example of digital  
1177 image analysis of EdU-positive nuclei (green) in iPSC cultures. Nuclei were also stained with  
1178 Hoechst 33342 dye (blue). Segmentation of the original microscopic image by Columbus  
1179 software is shown from left to right (all nuclei, valid nuclei, EdU-positive and valid nuclei). (B)  
1180 A trend towards increased proliferation is visible in heterozygous CUL3 KO (+/-) iPSC cultures  
1181 compared to isogenic wildtype (+/+) control cultures (left histogram). A significant increase in  
1182 proliferation is detectable in heterozygous CUL3 KO (+/-) NPC cultures (right histogram).  
1183  $t(13.61) = 3.99$ ,  $**p \leq 0.01$ , unpaired Welch's t-test. Data from 3-4 cultures per clone are shown  
1184 in box-and whiskers plots. The box depicts the median and the 25th and 75th quartiles, and  
1185 the whiskers show the 5th and 95th percentile. Scale bar represents 100  $\mu\text{m}$ .

1186

1187 **Fig. 5.** (A) Histograms showing increased mRNA expression of the NPC marker PAX6 in NPC  
1188 cultures of heterozygous CUL3 KO clones 6 and 19 (black bars), as detected by PCR array  
1189 analysis (left panel) and qRT-PCR (right panel), respectively.  $**p \leq 0.01$ ,  $***p \leq 0.001$ , unpaired  
1190 Welch's t-tests. (B) Histograms showing increased mRNA expression of SLC1A3, a marker for  
1191 radial glia cells and NPCs, in iPSC-derived neuron cultures from heterozygous CUL3 KO  
1192 clones 6 and 19 (black bars), as detected by PCR array analysis (left panel) and qRT-PCR  
1193 (right panel), respectively.  $**p \leq 0.01$ ,  $****p \leq 0.0001$ , unpaired Welch's t-tests. (C)  
1194 Immunostaining of NPC cultures and digital image analysis reveal significantly increased  
1195 numbers of strongly Pax-6 immunofluorescent cells (green) in heterozygous CUL3 KO clones  
1196 6 and 19, whereas Nestin immunofluorescence (red) is unchanged.  $**p \leq 0.01$ , unpaired  
1197 Welch's t-tests. Quantitative RT-PCR and image analyses were performed using three cultures  
1198 per clone. Histograms show mean  $\pm$  SEM, and data points superimposed on the bars.  
1199 Additional information on statistical analysis is given in Supplementary Table S2.

1200

1201 **Fig. 6.** Analysis of spontaneous electrical activity of iPSC-derived neurons using multi-  
1202 electrode array (MEA) recordings. Human iPSC-derived neurons were dot-seeded onto 24-  
1203 well, glass-bottom MEA plates following differentiation into cortical glutamatergic neurons  
1204 either by small molecules (A) or by lentiviral NGN2 expression (B, C). (A) Wildtype iPSC-

1205 derived neurons did not show a significant change in spontaneous activity from div 12 to div  
1206 23 after seeding, whereas heterozygous CUL3 KO clones 6 and 19 show a significant  
1207 decrease in activity over time. \*\*\*\* $p \leq 0.0001$ , unpaired Welch's t-tests. The inset shows two  
1208 neural rosettes (encircled) near an electrode (black) detected by bright field microscopy of the  
1209 MEA plate. (B) Following NGN2-mediated direct neuronal conversion from iPSC, both wildtype  
1210 iPSC-derived neurons and heterozygous CUL3 KO neurons exhibit a steady increase in  
1211 spontaneous electrical activity during neuronal maturation. Data are shown in box-and  
1212 whiskers plots. The box depicts the median and the 25th and 75th quartiles, and the whiskers  
1213 show the 5th and 95th percentile. Detailed data analysis of (B) is shown in (C). (C) Multi-  
1214 parametric analysis of spontaneous spikes, bursts, and network bursts during MEA recordings  
1215 of induced wildtype neurons (from iPSC clones CB4, 2, and 13) and induced heterozygous  
1216 CUL3 KO neurons (from clones 6 and 19) at various time-points (div 14, div 20, and div 27)  
1217 after seeding onto MEA plates. a: spike rate (Hz); b: burst count; c: mean burst duration (s); d:  
1218 mean burst spike count; e: mean burst spike rate (10Hz); f: spikes in bursts (%); g: mean  
1219 interburst interval (s); h: spikes in network bursts (%). All parameters analyzed did not  
1220 significantly differ between heterozygous CUL3 KO and wildtype neuron cultures following  
1221 direct neuronal conversion from iPSC. Data from two independent MEA experiments, each  
1222 comprising three cultures per clone. Additional information on statistical analysis is given in  
1223 Supplementary Table S2.

1224

1225 **Fig. 7.** Immuofluorescent stainings for the neuron marker Map-2 (white) and the NPC marker  
1226 Pax-6 (green) in neuron cultures derived from iPSCs. Human iPSCs were differentiated into  
1227 cortical glutamatergic neurons using either small molecules (A, B), or lentiviral overexpression  
1228 of Neurogenin-2 (NGN2) (C, D). Representative microscopic images show large clusters  
1229 (neural rosettes) of Pax-6 positive NPCs in heterozygous CUL3 KO neuron cultures from clone  
1230 6 following small molecule-mediated neuronal differentiation (A), but not following NGN2-  
1231 mediated direct neuronal conversion (C). Exclusively Map-2 positive neurons are visible in  
1232 wildtype control cultures from clone CB4, as expected (B, D). Scale bars represent 100  $\mu\text{m}$ .  
1233 Overview images and quantitative analysis are shown in Fig. 8.

1234

1235 **Fig. 8.** Immuofluorescent stainings for the neuron marker Map-2 (red) and nuclear labeling  
1236 using Hoechst 33342 dye (blue). Human iPSCs were differentiated into cortical glutamatergic  
1237 neurons using small molecules. Representative composite microscopic images from Opera  
1238 Phenix imaging system show numerous radial-symmetric neural rosettes in heterozygous  
1239 CUL3 KO neuron cultures from clones 6 and 19. Exclusively Map-2 positive neurons are visible  
1240 in wildtype control cultures. Scale bar represents 100  $\mu\text{m}$ . Quantitative analysis of the number

1241 of neural rosettes per region of interest (ROI) is shown in the box-and whiskers plot. The box  
1242 depicts the median and the 25th and 75th quartiles, and the whiskers show the 5th and 95th  
1243 percentile. \*\*\*\* $p \leq 0.0001$ , Kruskal Wallis test followed by pairwise Mann-Whitney U tests. Five  
1244 ROIs per well and 10 wells per clone were analyzed. Additional information on statistical  
1245 analysis is given in Supplementary Table S2.

1246

1247 **Fig. 9.** High-content image analysis of synaptic puncta labeled by the presynaptic marker,  
1248 synapsin 1/2 (Syn-1/2), and the postsynaptic marker, postsynaptic density protein 95 (Psd-95),  
1249 which are located close to Map-2 positive dendrites. (A, upper row) Detection of Map-2  
1250 immunoreactive (red) valid dendrites, and Syn-1/2 immunopositive (green) presynaptic puncta  
1251 by Columbus software. (A, lower row) Representative microscopic images showing Psd-95  
1252 (green, left), vGlut-1 (green, right), and Map-2 (red) immunofluorescent signals. Scale bars  
1253 represent 50  $\mu\text{m}$ . (B) A significant reduction in Syn-1/2 positive, presynaptic puncta per  
1254 micrometer neurite is detected in cultures from heterozygous CUL3 KO clones 6 and 19  
1255 compared to isogenic wildtypes. \*\*\*\* $p \leq 0.0001$ , unpaired Welch's t-tests. (C) The density of  
1256 Psd-95 positive, postsynaptic puncta does not significantly differ between genotypes. 90-130  
1257 regions of interest per well, and 4 wells per clone were analyzed. Data are shown in box-and  
1258 whiskers plots. The box depicts the median and the 25th and 75th quartiles, and the whiskers  
1259 show the 5th and 95th percentile. Additional information on statistical analysis is given in  
1260 Supplementary Table S2.

1261

1262 **Fig. 10.** Analysis of evoked electrical activity of NGN2-induced neurons using MEA recordings  
1263 and calcium imaging, respectively. (A) Exposure of channelrhodopsin-2 expressing, induced  
1264 neurons on MEA plates to ten blue light pulses evokes time-locked electrical spikes as shown  
1265 by representative raster plots from isogenic wildtype clone CB4 and heterozygous CUL3 KO  
1266 clone 6, respectively. The blue lines indicate light ON. At the highest light intensity (5 mA)  
1267 evoked activity in CUL3 KO neuron cultures declines after 5 light pulses. (B) The increase in  
1268 spike rate following optogenetic stimulation is significantly smaller in heterozygous CUL3 KO  
1269 neuron cultures from clones 6 and 19 compared to isogenic WT control clones. \*\* $p \leq 0.01$ , \*\*\* $p$   
1270  $\leq 0.001$ , unpaired Welch's t-tests. (C) Electrical stimulation and calcium imaging of NGN2-  
1271 induced neurons using a fluorometric imaging plate reader provides consistent results. A  
1272 significant decrease in excitability of heterozygous CUL3 KO neurons from clones 6 and 19 is  
1273 visible at increasing stimulus intensity, when compared to isogenic control clones. \*\*\*\* $p \leq 0.001$ ,  
1274 unpaired Welch's t-tests. Data are from 4-6 cultures per clone. Graphs depict mean  $\pm$  SEM.  
1275 Additional information on statistical analysis is given in Supplementary Table S2.

1276



1277 **Fig. 11.** (A, upper panel) Representative immunoblots showing similar levels of the putative  
1278 Cullin-3 substrate RhoA in heterozygous CUL3 KO iPSCs and NPCs, respectively, compared  
1279 to isogenic WT control cultures. (A, lower panel) Total protein stain confirms similar protein  
1280 loading. M, protein markers (colorimetric detection); +/+\_4, wildtype, parental control iPSC line  
1281 CB4; +/+\_2 and +/+\_13, Cas9/gRNA-transfected, non-edited, wildtype iPSC clones 2 and 13,  
1282 respectively; +/-\_6 and +/-\_19, Cas9/gRNA-transfected, heterozygous CUL3 knockout (KO)  
1283 clones 6 and 19, respectively. (B) Analysis of target gene expression of FGFR/MAPK signaling  
1284 in NPC cultures. Messenger RNA levels of the feedback inhibitors SPRY1 and IL17RD/SEF  
1285 are significantly lower in heterozygous CUL3 KO NPCs. \*\* $p \leq 0.01$ , unpaired Welch's t-tests.  
1286 Data from 5-8 NPC cultures per clone are shown in box-and whiskers plots. The box depicts  
1287 the median and the 25th and 75th quartiles, and the whiskers show the 5th and 95th percentile.  
1288 Additional information on statistical analysis is given in Supplementary Table S2.

### 1289 Highlights

- 1290 • Heterozygous CUL3 knockout (ko) iPSC and isogenic control lines were generated using  
1291 CRISPR/Cas9 nickase
- 1292 • Neuronal differentiation by small molecules showed delayed transition from radial glia to  
1293 neurons in CUL3 ko cultures
- 1294 • Direct neuronal conversion of CUL3 ko iPSC by lentiviral Ngn-2 overexpression obscured  
1295 delayed neuronal differentiation
- 1296 • Evoked neuronal activity is decreased in Ngn2-induced neurons from CUL3 ko iPSC, while  
1297 spontaneous activity is unchanged
- 1298 • FGF signaling is affected in CUL3 knockout neural precursor cells, while RhoA and Notch  
1299 signaling is unaltered



